

1 Evolution of the Iberian Massif as deduced from its crustal thickness and 2 geometry of a mid-crustal (Conrad) discontinuity

3 Puy Ayarza¹, José Ramón Martínez Catalán¹, Ana Martínez García², Juan Alcalde², Juvenal Andrés^{1,2},
4 José Fernando Simancas³, Immaculada Palomeras¹, David Martí^{2,4}, Irene DeFelipe², Chris Juhlin⁵,
5 Ramón Carbonell²

6 1. Geology Department, Salamanca University. Pza de la Merced, s/n. Salamanca 37008. Spain

7 2. Geosciences Barcelona, CSIC. Lluís Solé i Sabaris, s/n. Barcelona 08028. Spain

8 3. Geodynamics Department, Granada University. Av/ de la Fuente Nueva, s/n. Granada 18071. Spain

9 4. Lithica SCCL. Avinguda Farners 16, Santa Coloma de Farners, Girona 17430. Spain

10 5. Department of Earth Sciences, Uppsala University. Villavägen 16, Uppsala, 75236. Sweden

11
12 Corresponding author: Puy Ayarza (puy@usal.es)

13 Abstract

14 Normal incidence seismic data provide the best images of the crust and lithosphere. When
15 properly designed and continuous, these sections greatly contribute to understanding the
16 geometry of orogens and, together with surface geology, to unravel their evolution. In this
17 paper we present the most complete transect, to date, of the Iberian Massif, the westernmost
18 exposure of the European Variscides. Despite the heterogeneity of the dataset, acquired
19 during the last 30 years, the images resulting from reprocessing with a homogeneous workflow
20 allow us to clearly define the crustal thickness and its internal architecture. The Iberian Massif
21 crust, formed by the amalgamation of continental pieces belonging to Gondwana and
22 Laurussia (Avalonian margin), is well structured in upper and lower crust. A conspicuous mid-
23 crustal discontinuity is clearly defined by the top of the reflective lower crust and by the
24 asymptotic geometry of reflections that merge into it, suggesting that it has often acted as a
25 detachment. The geometry and position of this discontinuity can give us insights on the
26 evolution of the orogen, i.e. of the magnitude of compression and the effects and extent of
27 later Variscan gravitational collapse. Also, the limited thickness of the lower crust below, in
28 central and NW Iberia, might have constrained the response of the Iberian microplate to
29 Alpine shortening. This discontinuity, featuring a Vp increase, is here observed as an orogen-
30 scale boundary with characteristics compatible with those of the worldwide debated, Conrad
31 discontinuity.

32 **Keywords:** Iberian Massif, vertical incidence seismic data, mid-crustal detachment, Conrad
33 discontinuity, geodynamic evolution

34 Glossary:

35 CIA: Central Iberian Arc

36 CIZ: Central Iberian Zone

37 CU: Central Unit

38 CZ: Cantabrian Zone

39 DB: Duero Basin

40 GTMZ: Galicia Tras-os-Montes Zone

41 IAA: Ibero-Armorican Arc

42 ICS: Iberian Central System
43 NI: Normal Incidence
44 OMA: Ossa-Morena Zone
45 SPZ: South Portuguese Zone
46 TB: Tajo Basin
47 WA: Wide Angle
48 WALZ: West Asturian-Leonese Zone

49 **1. Introduction**

50 In the last 35 years, controlled source seismic data have greatly contributed to the
51 understanding of the European Variscides. National research programs like DEKORP (Bortfeld,
52 1985; DEKORP Research Group, 1987; Franke et al., 1990; Oncken, 1998), BIRPS and ECORS
53 (BIRPS and ECORS, 1986) have sampled this orogen providing a detailed picture of its
54 lithospheric architecture. In the Iberian Massif, normal incidence (NI) seismic reflection profiles
55 often acquired with coincident wide angle (WA) reflection/refraction seismic data have
56 allowed scientists to depict its crustal structure, infer its P and S-wave velocity distribution,
57 place constraints on its geodynamic evolution, visualize the accommodation pattern of
58 shortening at different crustal levels and, sometimes, deduce the effect of Alpine reactivation
59 on this Paleozoic orogen.

60 In this regard, seismic datasets acquired in the Iberian Massif (DeFelipe et al., 2020) within the
61 ESCIN (Ayarza et al., 1998, 2004; Pérez-Estaún et al., 1991; Pulgar et al., 1996), IBERSEIS
62 (Flecha et al., 2009; Palomeras et al., 2009; Simancas et al., 2003), ALCUDIA (e.g., Ehsan et al.,
63 2014, 2015; Martínez Poyatos et al., 2012) and CIMDEF projects (Andrés et al., 2019) have
64 helped to identify several outstanding features such as i) clear differences in the intensity and
65 geometry of reflectivity at upper and lower crustal levels, ii) contrasting deformation patterns
66 deduced from the good correlation between reflectivity and upper crustal structures as,
67 regardless of the many factors that trigger the concentration of deformation along narrow
68 thrust zones (Butler and Mazzoli, 2006), the latter often follow lithological boundaries in the
69 Iberian Massif (e.g., Alonso, 1987), thus being candidates to appear as outstanding reflections,
70 and iii) a very reflective and sometimes thick lower crust, even in areas where the upper crust
71 is weakly deformed. In order to explain these features, decoupling of the upper and lower
72 crust, eased by a mid-crustal detachment, has been invoked along large parts of the sampled
73 area (Simancas et al., 2013). However, coupled crustal deformation has been inferred in NW
74 Iberia, where large crustal thickening took place. Also, no inference has been made on how
75 this detachment acted during later Alpine deformation in the central and northern Iberian
76 Massif.

77 In this paper, we present a new composite seismic section of the Iberian Massif that integrates
78 results of two new datasets: CIMDEF and ALCUDIA WA. The former fill the gap between areas
79 previously unexplored, like Central Iberia, thus contributing to provide an almost complete
80 transect. In addition, we include the N-S, ESCIN-2 seismic profile and new time-migrated
81 sections of all datasets, some of them, as yet, unmigrated (e.g., ESCIN-1). Although the
82 detailed interpretation of the upper crustal reflectivity and its correlation with the surface
83 geology does not significantly change, we revisit the deep reflectivity and redefine the

84 extension and implications of a mid-crustal discontinuity that, in our view, exists below the
85 entire Iberian Massif, affecting the two continents involved in the Variscan Orogeny and
86 certainly playing a critical role in the decoupling between upper and lower crustal
87 deformation. Finally, we infer the geometry and nature of this feature, discuss its tectonic
88 significance and its role during the younger Alpine Orogeny, and relate it with the long-
89 debated (e.g., Finlayson et al., 1984; Litak and Brown, 1989; Wever, 1989; Xiaobo and Tae
90 Kyung, 2010) Conrad discontinuity (Conrad, 1925) of the classic continental seismology.

91 **2. Geological setting**

92 The Iberian Massif represents the westernmost outcrop of the European Variscides, exposing
93 an almost complete section of this Paleozoic orogen. It is divided into six zones (Fig. 1; Arenas
94 et al., 1988; Farias et al., 1987; Julivert et al., 1972) that from N to S and E to W are: Cantabrian
95 (CZ), West Asturian-Leonese (WALZ), Galicia-Tras-os-Montes (GTMZ), Central Iberian (CIZ),
96 Ossa-Morena (OMZ) and South Portuguese (SPZ). The CZ and the SPZ represent external zones
97 whereas the rest represent the hinterland. The CZ, WALZ and CIZ belong to the northern
98 margin of the Paleozoic Gondwana. The GTMZ represents the remnants of a large nappe stack
99 formed by pieces of the outermost Gondwana margin, i.e., a pulled-apart peri-Gondwanan
100 terrane and ophiolitic units derived from the Rheic oceanic realm separating them. The OMZ
101 has been interpreted as a continental fragment that rifted and probably drifted away from
102 Gondwana (Matte, 2001; Robardet, 2002), docking back later to the CIZ giving rise to a suture
103 (Azor et al., 1994; Gómez-Pugnaire et al., 2003; Simancas et al., 2001). Finally, the SPZ is
104 thought to be separated from the OMZ also by the Rheic Ocean suture (Simancas et al., 2003)
105 which was later overprinted by early Carboniferous extension (Azor et al., 2008) and by
106 transpression (Pérez-Cáceres et al., 2015). In this context, the basement of the SPZ represents
107 a fragment of Avalonia (Braid et al., 2011, 2012; Pereira et al., 2014; Rodrigues et al., 2015),
108 and its affinity with the Rheno-Hercynian Zone in Germany (Franke, 2000; Franke et al., 1990)
109 further supports this correlation.

110 From a tectonic point of view, the Iberian Massif shows evidence of pre-Variscan activity. The
111 Cadomian Neoproterozoic event is characterized by continental arc magmatism, deformation
112 and metamorphism (Bandrés et al., 2004; Dallmeyer and Quesada, 1992; Ochsner, 1993). It
113 developed above a previous non-outcropping continental crust, and formed the basement
114 above which the Ediacaran and Paleozoic sedimentation took place, favored by Ediacaran-
115 Cambrian and Cambro-Ordovician rifting which developed a wide continental platform
116 (Linnemann et al., 2008; Sánchez-García et al., 2008, 2010). However, most of the outcropping
117 tectonic features are the result of the Devonian and Carboniferous collision between
118 Gondwana, some peri-Gondwanan terranes and the Avalonian border of Laurentia, which
119 resulted in the Variscan Orogen (Matte, 2001). The deformation associated to the latter was
120 diachronous along the Iberian Massif. Next, we describe the most important tectonic and
121 stratigraphic features of this part of the European Variscides, by tectonic zones and from N to S
122 (in present coordinates).

123 **2.1. Cantabrian Zone (CZ)**

124 The CZ (Fig. 1) is an external zone located at the core of the Ibero-Armorican Arc (IAA; Dias and
125 Ribeiro, 1995; Lotze, 1929; Matte and Ribeiro, 1975; Stille, 1924). It is a thin-skinned thrust and

126 fold belt with a transport direction towards the foreland to the E, and overprinted by the
127 oroclinal folding giving rise to the IAA (Alonso et al., 2009; Pérez-Estaún et al., 1988).
128 Stratigraphically, it is characterized by a Precambrian sequence, outcropping at its western
129 part and overlain by a Paleozoic stratigraphic succession that ranges from the Cambrian to a
130 well-developed Carboniferous: pre-orogenic up to early Carboniferous, and syn-orogenic in the
131 Upper Carboniferous (Sánchez de Posada et al., 1990; Truyols et al., 1990). Scarce tholeiitic
132 and alkaline magmatism is related to Cambro-Ordovician rifting (Corretgé and Suárez, 1990).
133 No regional metamorphism accompanied deformation, indicating shallow crustal conditions. In
134 this area, deformation began at ~325-320 Ma, in the Late Mississippian (Dallmeyer et al.,
135 1997), and the emplacement of nappes that characterize the deformation and the formation
136 of folds took place between the Westphalian B and the Stephanian (313-300 Ma), in the Upper
137 Carboniferous (Pérez-Estaún et al., 1988). An extensional episode related to the end of the
138 orogeny led to the formation of Permian Basins (Martínez García, 1981). Later on, extension
139 related to the opening of the Bay of Biscay triggered the development of deep Cretaceous
140 basins (Quintana et al., 2015; Rat, 1988). Alpine tectonics uplifted the Pyrenean-Cantabrian
141 range from the end of the Late Cretaceous to the Miocene (DeFelipe et al., 2019; Teixell et al.,
142 2018 and references therein) reactivating Variscan thrusts and Mesozoic normal faults
143 (Gallastegui et al., 2016).

144 **2.2. West Asturias-Leonese Zone (WALZ)**

145 The WALZ lies to the W of the CZ (Fig. 1). Stratigraphically, it consists of a Neoproterozoic
146 terrigenous sequence unconformably overlain by a Paleozoic platform succession that ranges
147 from the Cambrian to the Lower Devonian (Pérez-Estaún et al., 1990), being much thicker than
148 that of the CZ. These sediments were actively deformed along three compressional (C1, C2,
149 and C3) and two extensional (E1 and E2) phases during the Variscan Orogeny (Martínez
150 Catalán et al., 2014). Large E vergent folds witness the C1 related compression (360-340 Ma).
151 Those were later affected by E vergence thrusts resulting from ongoing shortening (345-325
152 Ma). Crustal thickening followed by thermal relaxation led to syn-orogenic extension during E1
153 (330-315 Ma). A last compressional episode (C3, 315-305 Ma) produced upright folds
154 associated with wrench shear zones while simultaneous extension (E2, 315-300 Ma)
155 continued, characterizing the latest stages of the orogeny in this area. Crustal melting
156 triggered by compression and thickening (C1-C3) led to extension (E1-E2) and to the intrusion
157 of granitoids in the western part of the WALZ. Thermal models show that the crust could have
158 started to melt within 30 Ma after the onset of crustal thickening, which is then constrained by
159 the ages of Variscan granitoids (Alcock et al., 2009).

160 **2.3. The Central Iberian Zone (CIZ)**

161 The CIZ is the largest of the Iberian Massif zones. Curvature of magnetic anomalies and that of
162 early (C1) Variscan folds depict the Central Iberian Arc (CIA; Martínez Catalán, 2011a, 2011b),
163 partly explaining the width of this internal zone (Fig. 1). The stratigraphic sequence differs
164 from N to S: Ordovician felsic metavolcanic, subvolcanic and intrusives (Diez-Montes et al.,
165 2010) represent the most ancient lithologies outcropping in the N, defining the 'Ollo de Sapo'
166 domain whereas to the S, Upper-Proterozoic-Lower Cambrian metasediments outcrop (Díez
167 Balda et al., 1995), defining the 'Schist-Greywacke Complex' domain. The pre-orogenic

168 sedimentary sequence continues to the Devonian, followed by a syn-orogenic Carboniferous
169 sequence (Martínez Catalán et al., 2004; Robardet, 2002). This area represents a relatively
170 stable Gondwana margin characterized by the Early Ordovician extension that opened the
171 Rheic Ocean and allowed intrusion of the essentially felsic magmas of the Ollo de Sapo Fm.
172 (Díez Montes et al., 2010). The deformation phases described for the WALZ affected most of
173 the CIZ although C1, C2 and E1 are somewhat older, according to the propagation of
174 deformation from the hinterland. Slight differences in the importance of phases can also be
175 found to the center and S (Martínez Catalán et al., 2019), allowing the CIZ to be divided in two
176 zones. In the NW, intense recumbent C1 folds and important C2 thrusts related to the
177 emplacement of the GTMZ occur. Outcropping rocks show epi- to catazonal metamorphism
178 and ductile detachments. Gneiss domes of both E1 and E2 extensional phases exist, evidencing
179 significant crustal thinning, and Variscan granitoids are abundant. To the S, C1 folds are
180 upright, C2 deformation is limited to the southernmost part, and upright C3 folds are the most
181 important structures (Martínez Catalán et al., 2012; Martínez Poyatos, 2002). Metamorphism
182 is generally weak and the amount of granitoids decreases, except in the Iberian Central System
183 (ICS). Here extension postdates C3 upright folding and thus, it is considered E2. Alpine
184 tectonics in the CIZ reactivated previous Variscan fractures and triggered the development of
185 the Iberian Central System (ICS) mountain belt (de Vicente et al., 1996), allowing the products
186 of syn- and post-E2 crustal melting to outcrop in large areas.

187 **2.4. The Galicia-Tras-os-Montes Zone (GTMZ)**

188 The GTMZ is represented by five klippen that are remnants of the emplacement of a thick
189 nappe stack on top of the CIZ. This includes, from bottom to top, a relatively distal part of the
190 northern Gondwana margin (Parautochthon), the outermost edge of that margin (Lower
191 Allochthon), a few oceanic units of Cambro-Ordovician and Lower Devonian age (Middle
192 Allochthon) and a peri-Gondwanan terrane with magmatic evidences of Cambro-Ordovician
193 rifting and a continental arc setting (Upper Allochthon). Several units show high-P
194 metamorphism reflecting subduction of the ocean represented by the Middle Allochthon and
195 involving also the Upper and Lower ones (Arenas et al., 2007; Gómez Barreiro et al., 2007;
196 Martínez Catalán et al., 2007; Sánchez Martínez et al., 2007). Ongoing subduction during most
197 of the Devonian (400-365 Ma) built an accretionary wedge that was subsequently emplaced on
198 top of the CIZ during the early Carboniferous (C1-C2 events, 360-340 Ma).

199 **2.5. The Ossa-Morena Zone (OMZ)**

200 The boundary between the CIZ and the OMZ (the Badajoz Córdoba Shear Zone) has been
201 largely interpreted as a suture (Gómez-Pugnaire et al., 2003; Simancas et al., 2001), although
202 no true oceanic units have been identified. It includes amphibolites of oceanic affinity from the
203 early Paleozoic, as well as eclogite relics.

204 In general, SW Iberia features outcrops from the Upper Precambrian to the Upper
205 Carboniferous, with an angular unconformity at the Lower Carboniferous. In the OMZ, the
206 Serie Negra (Black Series) is a thick Neoproterozoic sequence that includes graphitic quartzites
207 and schists and underwent Cadomian arc-related magmatism and regional metamorphism
208 (Dallmeyer and Quesada, 1992; Ochsner, 1993; Quesada and Dallmeyer, 1994). The pre-
209 orogenic Paleozoic sequence is rather complete and was deposited at the peri-Gondwanan

210 platform, as for the CIZ, although differences in the faunal content and in the Paleozoic facies,
211 generally more pelitic in the OMZ, point to a more distal position (Robardet, 2002; Robardet
212 and Gutiérrez Marco, 1990). Ediacaran-Cambrian and Cambro-Ordovician magmatism reflects
213 two rifting events, the latter including alkaline magmatism related to the opening of the Rheic
214 Ocean (García Casquero et al., 1985; Ochsner, 1993; Sánchez-García et al., 2008, 2010). The
215 first deformation event, of Devonian age, formed overturned and recumbent folds and thrust
216 faults with SW vergence (Expósito et al., 2002, 2003). Syn-orogenic, early Carboniferous basins
217 developed in an extensional context and are related to calc-alkaline volcanism and magmatism
218 (Casquet et al., 2001). These deposits unconformably overlay early folds and thrusts. Later,
219 deformation continued with middle and upper Carboniferous sinistral transpression and
220 associated upright NW-SE folds.

221 A salient seismic reflector, the Iberseis Reflective Body (IRB, Carbonell et al., 2004; Simancas et
222 al., 2003), located along a mid-crustal detachment, seems to be a mantle-derived intrusion
223 emplaced during early Carboniferous extension (350-340 Ma). At this time, the hinterland to
224 the NW was undergoing the first stages of compression (C1-C2).

225 **2.6. The South-Portugese Zone (SPZ)**

226 The boundary between the OMZ and the SPZ has been long understood as a suture on the
227 basis of geometric assumptions (e.g., Carvalho, 1972). Later evidences have reinforced this
228 point of view suggesting that it represents the remnants of the Rheic Ocean, although
229 Carboniferous transtension and transpression have largely obliterated it (Pérez-Cáceres et al.,
230 2015 and references therein).

231 The SPZ is a Variscan foredeep basin strongly deformed by thin-skinned thrust tectonics, and is
232 usually correlated with the Rhenohercynian Zone of Kossmat (1927), in the Bohemian Massif.
233 It features wide outcrops of low or very low grade Devonian phyllites, quartzites and
234 sandstones overlain by a lower Carboniferous (Early Mississippian) volcano-sedimentary
235 sequence topped by middle and upper Carboniferous flysch (Oliveira, 1990). From a tectonic
236 point of view, it is characterized by Carboniferous S vergent thrusts and folds, the latter
237 featuring axial traces oblique to the northern boundary of the zone, evidencing transpression
238 (Simancas et al., 2003 and references therein). Deformation propagated towards the S during
239 the lower and upper Carboniferous (Oliveira, 1990).

240 Although the start of the Variscan collision seems to have been frontal or maybe right-lateral
241 in most of Europe (Shelley and Bossière, 2000), surface geology and interpretation of seismic
242 data evidences the existence of relevant left lateral transpression and oblique-slip syn-
243 metamorphic shear zones in the OMZ, SPZ and their boundaries (Pérez-Cáceres et al., 2016;
244 Simancas et al., 2003 and references therein). In the OMZ, folds and thrusts witnessing
245 Devonian and early Carboniferous compression are oblique to the OMZ/SPZ boundary,
246 indicating a transpressional setting. There, Devonian and Carboniferous left lateral
247 deformation accounts for ~400 km, higher than perpendicular shortening. Likewise, inside the
248 SPZ, left-lateral displacement is estimated to reach 90 km whereas the orthogonal one
249 amounts ~60 km (Pérez-Cáceres et al., 2016).

250 **3. Geophysical setting: Existing datasets, their reprocessing and a brief description**

251 **3.1. Seismic datasets sampling the Iberian Massif**

252 Since the early 1990s, the Iberian Massif has been sampled by different controlled source
253 seismic experiments (DeFelipe et al., 2020): the ESCIN (1991-1992), IBERSEIS (2000 and 2003),
254 and ALCUDIA (2007-2012) experiments acquired normal incidence (NI) and coincident wide-
255 angle (WA) data. The latest project, carried out with the target of understanding the structure
256 and effect of the Alpine reactivation across the central part of the Iberian Massif, is the
257 CIMDEF experiment (2017-2019). It recorded densely spaced controlled source WA reflection
258 and natural source (earthquakes and noise) seismic data. However, the acquisition of
259 coincident NI data along this transect has not currently been planned, regardless of its
260 potential quality and relevance, due to the relatively high costs of this kind of experiment.

261 From N to S, and from E to W, the ESCIN project sampled the northern part of the Iberian
262 Massif (Fig. 1). Profile ESCIN-1 (1991) is an onshore E-W line crossing the CZ from its eastern,
263 most external part to its boundary with the WALZ to the W; Profile ESCIN-2 (1991) is an
264 onshore N-S profile crossing the most external and eastern part of the CZ and reaching the
265 northern end of the Duero Basin (DB) to the S, which represents the Cantabrian Mountains
266 foreland basin. The ESCIN-3 (1992) profiles sampled the WALZ and the CIZ along the northern
267 Iberia shelf. Although it consists of three parts (ESCIN-3.1, 3.2 and 3.3) only the easternmost
268 ones (3.2 and 3.3.) are relevant for this study and thus, included here. ESCIN-3.3 crossed the
269 entire WALZ to its western boundary with the CIZ, which in this area was surveyed by the
270 ESCIN-3.2. Geographically, the latter also sampled the allochthonous GTMZ. But as this is an
271 offshore profile, it shows no evidences of the presence of the GTMZ, and most of the imaged
272 crust corresponds to that of its relative autochthon, the CIZ.

273 A significant geographical and methodological gap exists between the ESCIN profiles to the N
274 and the location of the CIMDEF experiment (Fig. 1). The latter crosses central Iberia from the N
275 part of the CIZ, then samples the DB down to the ICS, and goes on S across the Tajo Basin (TB)
276 till it reaches again the CIZ metasediments.

277 In the southern part of the Iberian Massif, the onshore ALCUDIA seismic line (NI and WA),
278 striking NE-SW, was acquired across the CIZ, going from the S of the ICS to the boundary with
279 the OMZ. Finally, the NE-SW IBERSEIS dataset (NI and WA) is also an onshore profile that
280 structurally overlaps the SW end of the ALCUDIA line although with some 50 km of offset to
281 the W. This seismic line samples the southern part of the CIZ, the OMZ and the SPZ.

282 Altogether these seismic profiles account for a ~1500 km long seismic transect geared to
283 understand the crustal and, in places, lithospheric structure of the Iberian Massif and to
284 constrain its evolution.

285 **3.2. Processing of datasets**

286 The data used in this work have been acquired at different times, have different characteristics
287 (onshore and offshore) and accordingly exhibit very heterogeneous quality. Table 1 shows
288 their acquisition parameters. The most outstanding differences are: i) the quality and
289 characteristics of the offshore (ESCIN-3) vs the onshore data, ii) the difference between the
290 low fold (30) ESCIN data, acquired with explosive sources and airguns, and the high fold (>60)

291 IBERSEIS and ALCUDIA datasets, which used Vibroseis trucks as source of energy, and iii) the
292 fact that the CIMDEF dataset lacks NI data and only provides lower resolution noise and
293 earthquake data, since WA profiles are, as yet, unpublished. Thus, reprocessing all NI data was
294 mandatory, at least at stack and post-stack level. Figure 2 shows the processing flow followed
295 to homogenize the display of datasets while preserving the true amplitude (Martínez García,
296 2019). The software package used for reprocessing was GLOBE Claritas
297 (www.globeclaritas.com/) and the most important steps were related to frequency filtering,
298 amplitude weighting and equalization, Kirchhoff time migration and coherency filtering (Fig. 2).
299 In addition, up to 20 multi-trace attribute analysis were tested with the goal to enhance
300 structural and lithological impedance contrasts that allowed to improve the interpretation
301 (Chopra and Alexeev, 2005; Taner and Sheriff, 1977). Although this methodology has been
302 mostly used in sedimentary reservoirs, we have seen that the application of these techniques
303 can enhance the continuity of reflections and help to identify different types of crust, thus
304 easing the interpretation. Some of the boundaries resulting from this attribute analysis (e.g.,
305 variance and chaos attribute filters, the former estimating the local variance in the signal and
306 the latter measuring the lack of organization in the reflectivity) are included in the
307 interpretations.

308 **3.3. Description of the seismic sections**

309 The NI datasets included in this paper have already been presented, so the reader will be
310 referred, in every sub-section, to previous publications that include detailed descriptions of
311 pre-stack processing and interpretations. Here we will just focus on those features that are
312 essential to our interpretation.

313 Geological cross-sections coincident with reprocessed time-migrated sections and their
314 interpretations are presented in figure 3 (ESCIN-1), figure 4 (ESCIN-2), figure 5 (ESCIN-3.3),
315 figure 6 (ESCIN-3.2), figure 7 (ALCUDIA), and figure 8 (IBERSEIS). Migration velocities (Fig. 2) are
316 average crustal values as calculated from coincident or nearby WA models. Depth conversion
317 using migration velocities is also carried out. The description of sections will be done from N to
318 S and from E to W. The CIMDEF dataset will be only described in the discussion (Figs. 9 and 10)
319 as it does not include NI data but is key to understanding the geometry of the mid-crustal
320 discontinuity, its late Variscan reworking and its Alpine reactivation.

321 **3.3.1. Cantabrian Zone (ESCIN-1 section)**

322 The ESCIN-1 section is a ~130 km long, E-W profile crossing the CZ from its most external part
323 to the Narcea Antiform to the W, in the boundary with the hinterland (WALZ, Figs. 1 and 3).
324 The section, migrated at $v=5600$ m/s (Fig. 2) and its interpretation are presented in figure 3.

325 This profile was first described and interpreted over an unmigrated image by Pérez-Estaún et
326 al. (1994). Later works revisited the interpretation, adding travel-time modeling to help on the
327 understanding of the unmigrated data (Gallastegui et al., 1997). The reader is referred to these
328 papers for further details than those provided here.

329 In the upper crust, the western part shows W-dipping reflections that represent the Variscan
330 imbrication, through a thrust ramp (t in Fig. 3), of the basement under the Paleozoic

331 succession, indicating the proximity of the hinterland (WALZ). In fact, a Neoproterozoic, non-
332 metamorphic sequence outcrops in this area, which is probably underlain by an older
333 crystalline basement. Another prominent W-dipping reflection roughly parallel to t (t')
334 crosscuts subhorizontal ones, defining a pattern that might be providing an out of the plane
335 image of the above mentioned thrust ramp, as this profile lies in the hinge of an arcuate
336 structure, the IAA (Fig. 1b). To the E, the thin skinned tectonics characteristic of this external
337 zone can be interpreted from shallow subhorizontal to W dipping reflections often coincident
338 with outcropping thrusts (ot), as observed in figure 3a. The main one among these, running at
339 around 5 s (TWT), is interpreted as the sole thrust of the thin-skinned orogenic wedge (st). To
340 the W, it gets involved in the crustal ramp (t in Fig. 3) observed at the Narcea Antiform,
341 suggesting that it ends down rooting into the upper part of the lower crust (c). A low
342 reflectivity wedge of undifferentiated basement (b) located between 4-5 and 8.5 s (TWT) exists
343 underneath the easternmost reflections. This may image some pre-Paleozoic basement that is
344 interpreted as upper crust, since the pattern of reflections changes below, suggesting that a
345 significant boundary occurs underneath.

346 The lower crust shows little reflectivity but seems to be present in the interval between 8.5-14
347 s (TWT) in the E and between 8.5 and 12 s (TWT) in the W. It features subhorizontal (ir) and W
348 dipping internal reflectivity to the E, the latter (ir') crosscutting the former reflections. These
349 might represent the imprint of Alpine tectonics over a previously deformed/reflective lower
350 crust. To the W, reflectivity seems to be subhorizontal or dipping to the E (ir). Some of the
351 dipping and arcuated reflectivity observed at the edges of section ESCIN-1 (mig in Fig.3 and
352 thereafter) might be related to the migration effects over discontinuous features and caution
353 should be taken when interpreting it.

354 The Moho along this section (m) is located at nearly 14.5 s TWT (~45 km) in the eastern part,
355 and shallower (12 s TWT, ~36 km) to the W. The crustal thickening observed to the E is
356 probably related to an out of section image of the crustal Alpine root, better observed in
357 profile ESCIN-2, which is described next.

358 **3.3.2. Cantabrian Zone and Duero Basin (ESCIN-2 section)**

359 The ESCIN-2 seismic line is a 65 km long, N-S section that samples the transition between the
360 CZ and the DB (Fig. 1). Even though this profile was geared to study the Alpine structures, it
361 shows how the Variscan features have been reactivated during the Cenozoic compression
362 between the Iberian Peninsula and the European plate. The section was first presented by
363 Pulgar et al. (1996). Later on, some authors have used this image to constraint the Alpine
364 structure in the North Iberian Margin (e.g., Fernández-Viejo et al., 2000; Gallastegui et al.,
365 2016). However, only Teixell et al. (2018) used a migrated version (4000 m/s) of this section.
366 Here we present the results of a Kirchhoff time migration at $v=5600$ m/s (Fig. 4).

367 This seismic line shows, in places, a conspicuous reflectivity that allows a straightforward
368 interpretation. To the S end, the upper crust is characterized by high amplitude horizontal
369 reflectivity representing the DB sedimentary sequence (Fig. 4a). It occupies the interval from 0-
370 3.5 s TWT (s in Fig. 4b, c and d) and appears to be offset by N dipping reflections (t). The latter
371 have been interpreted as S vergent Alpine thrusts affecting the CZ basement and partly the DB
372 sediments. The rest of the crust is less reflective although N dipping reflectivity (ot), also

373 interpreted as Alpine thrusts on the basis of the clearer stack image (Pulgar et al., 1996),
374 crosscuts shallow subhorizontal weak reflections that represent the Paleozoic sedimentary
375 sequence of the CZ (ps).

376 The lower crust presents higher amplitude reflectivity. In general, a thick band of horizontal
377 reflections located between 7.5 and 12 s (TWT) at the southern part of the profile, bends and
378 dips to the N in the northern part of the line (lc) in response to Alpine compression. Although
379 the stacked section shows that this N dipping reflectivity reaches 14.5 s TWT (Pulgar et al.,
380 1996) the migrated sections (Teixell et al., 2018 and Fig. 4) indicate that these reflections move
381 southward and upward to less than 14 s (TWT), while losing amplitude and coherence. In fact,
382 the geometry of the bottom of the lowermost crust (Moho, m) is deduced on the basis of the
383 geometry of its uppermost part (c), the lower crust internal reflectivity, the stack image (Pulgar
384 et al., 1996), and the amplitude contrasts observed in the attribute analysis (Fig. 4).
385 Furthermore, its depth is solely established on the basis of the position of the strongest
386 subhorizontal reflections to the S.

387 Even though this profile shows the imprint of recent Alpine shortening, no reflections are
388 observed to crosscut the entire crust. In contrast, reflectivity suggests that deformation is
389 decoupled between the upper and lower crust. However, this section is not long and/or
390 reflective enough as to image where the Alpine thrusts (ot) root. Possibly, they merge into the
391 roof of the underthrust CZ lower crust.

392 A 1D Vp profile (Fig. 4e) extracted from the coincident WA model (Pulgar et al., 1996) shows a
393 conspicuous velocity increase in the lower crust, at a depth roughly coincident with (c). Depth
394 misfits are due to the effect of the low Vp of the DB sediments not being taken into account in
395 the depth conversion.

396 **3.3.3. West Asturian-Leonese Zone (ESCIN-3.3 section)**

397 The ESCIN-3.3 profile is part of a ~375 km long crooked offshore seismic line consisting in
398 ESCIN-3.1, 3.2 and 3.3. The latter is 137 km long, parallel to the coast and close to it across the
399 WALZ (Fig. 1). It was first presented by Martínez Catalán et al. (1995) and Ayarza et al. (1998,
400 2004). Later on, its image has been used to constrain the structure of the western North
401 Iberian Margin and that of the transition between the WALZ and the CIZ (Martínez Catalán et
402 al., 2012, 2014). The cross-section in figure 5a represents the onshore transect of this profile.

403 Reflectivity in the upper crust is characterized by the image of Mesozoic sedimentary basins (s
404 in Fig. 5) related to the extension that led to the opening of the Bay of Biscay. Underneath, W
405 dipping reflections (t) are interpreted as the imprint of the first stages of Variscan
406 compressional deformation in the WALZ (C1 and C2), developing E-vergent thrust faults (Fig.
407 5a). These affect the pre-Paleozoic basement and root in the upper part (c) of a thick reflective
408 band interpreted as the lower crust (lc) or in a sole thrust (st) that also reaches the lower crust.

409 The lower crust (lc) is represented by a thick band of subhorizontal reflectivity (8-12 s TWT)
410 that thickens (6-12 s TWT) in the westernmost part of the WALZ (CDP 3000) underneath the
411 Lugo Dome, an extensional structure bounded to the E by the Viveiro normal fault (Fig. 5).
412 Then it thins towards the end of the line, when entering the CIZ, coinciding with an area of E

413 dipping sub-crustal reflections (sc) altogether defining a less clear Moho (m) in this area. The
414 ESCIN-3.3 lower crust seems to feature an internal layer with mantle P-wave velocities when
415 modeled from coincident WA data. Accordingly it was interpreted as consisting of the WALZ
416 lower crust underthrust by the CZ lower crust (Ayarza et al., 1998). This model would
417 compensate the high shortening observed in the upper crust of the CZ, a thin-skinned belt
418 whose sole thrust roots at the contact with the WALZ. The internal reflectivity of the lower
419 crust shows W dipping reflectors (ir), similar to the ones observed in the upper crust and
420 probably imaging Variscan deformation in the lower crust, either compressional or
421 extensional. They crosscut subhorizontal reflectivity, thus postdating it. A 1D P-wave velocity
422 profile (Fig. 5e) derived from coincident WA data (Ayarza et al., 1998) shows again an
423 important increase in relation to the top of the lower crust (c).

424 Even though migration ($v= 5200$ m/s, Fig. 2) over discontinuous reflections blurs the seismic
425 section in the edges (mig in Fig. 5), reflectivity never seems to cross-cut the crust and/or the
426 Moho, indicating that deformation is decoupled at upper and lower crustal level. Subcrustal E
427 dipping reflections (sc) are interpreted as the out-of-the-plane image of the Alpine southward
428 subduction of the Bay of Biscay oceanic crust (Ayarza et al., 1998, 2004), which is out of the
429 scope of this paper.

430 The boundary between the WALZ and the CIZ is the Viveiro Fault, one of the most striking
431 surface expressions of Late Variscan extensional tectonics, featuring a decompression of ~ 4 kb
432 or 14 km (Reche et al., 1998). To its W, gravitational collapse of a thickened crust and
433 associated crustal extension and melting have played a key role in the orogenic evolution of
434 the CIZ. However, to the E, crustal re-equilibration after C1 and C2 thickening was less
435 important and igneous activity decreases. Even though this fault itself is not identified in the
436 seismic section (Fig. 4), the reflectivity in general varies to both sides of it, featuring a thinner
437 (9 s TWT vs 12 s TWT) and more transparent crust to the W (Fig. 6). In fact the geometry of
438 some reflections (ef) in the boundary between the WALZ and the CIZ, above the thickest lower
439 crust, and the subtractive way the sole thrust (st) merges with the lower crust (st') seem to
440 indicate the effect of extensional tectonics, sometimes reactivating compressional structures
441 (st-st'). Such a reactivation has been described on the basis of structural and metamorphic
442 considerations of the main WALZ thrust sheet (Alcock et al., 2009). Conversely, further to the
443 E, reflectivity probably represents the geometry of preserved compressional deformation.

444 **3.3.4. Northern Central Iberian Zone (ESCIN-3.2 section)**

445 The seismic line ESCIN-3.2 is a 97 km long profile, also parallel and close to the coast, that
446 samples the relative autochthon to the GTMZ, i.e. the CIZ (Figs. 1 and 6). It was first described
447 by Álvarez-Marrón et al. (1996) and later by Ayarza et al. (2004). Here it is presented migrated
448 at $v=5200$ m/s (Fig. 2). The cross-section in figure 6a corresponds to the equivalent onshore
449 transect of this profile and depicts allochthonous sequences not imaged by the NI data.

450 This profile shows, in the upper part, a band of high subhorizontal reflectivity that coincides
451 with the location of Mesozoic basins, as in profile ESCIN-3.3 (s in Fig. 6). The rest of the upper
452 crust is not very reflective although a couple of W-dipping reflections (ef) rooting in a thin
453 band of strong reflectivity are observed. These reflections, located in the E of the section from
454 4.5 s to 8 s TWT, define a sort of duplex, extensional or compressional, but later extended,

455 indicating in any case boudinage and crustal thinning. To the W, the upper crust is very
456 transparent and just a few weak reflections can be observed.

457 The narrow reflective band at 8-9 s TWT represents the lower crust (lc), and is the most
458 striking feature of this profile. Its 1 s TWT thickness contrasts with that observed in the
459 neighboring ESCIN-3.3 and ESCIN-1 sections, which show a much thicker lower crust (4-5 s
460 TWT). Reflectivity in this band is subhorizontal, although somewhat undulated, while the band
461 itself is slightly inclined to the W. In the E, the Moho (m) is located above 9 s TWT, the
462 shallowest identified so far in the Iberian Massif. Subcrustal E dipping reflections (sc) are again
463 associated to the 3D image of the southward subduction of the oceanic crust of the Bay of
464 Biscay during the Alpine convergence (Ayarza et al., 2004) whereas W dipping features might
465 be related with the CZ lower crust (czlc) underthrust also underneath the easternmost part
466 of the CIZ.

467 This profile samples the northern CIZ, where Variscan crustal thickening during C1 and C2, was
468 most important. Consequently, later gravitational collapse triggered extensional tectonics and
469 crustal melting, allowing the intrusion of granites and the development of extensional
470 detachments (with associated metamorphic offsets). The image of line ESCIN-3.2 shows a
471 transparent upper crust to the W suggesting that granites occupy most of it, which is
472 supported by onland geological mapping. Some thrust faults, as those imaged by W-dipping
473 reflections in profile ESCIN-3.3, probably root along this section and are represented by the W-
474 dipping reflections at the base of the upper crust. However, these were later flattened and/or
475 reactivated as extensional detachments by crustal thinning (ef). The narrowness of the highly
476 reflective lower crust here suggests that crustal thinning was largely accommodated at this
477 level, as the upper crust has basically the same thickness as in the ESCIN-3.3 line (up to 6-7 s
478 TWT). In addition, crustal melting might have also affected the top of the lower crust. But even
479 though large parts of the crust were melted, reflectivity exists deep in the upper crust,
480 suggesting that crustal melting was not pervasive and/or reflectivity is linked to syn- or late-
481 tectonic features.

482 **3.3.5. Southern Central Iberian Zone (ALCUDIA section)**

483 The ALCUDIA seismic profile was first presented by Martínez Poyatos et al. (2012) and
484 reprocessed and further interpreted by Ehsan et al. (2014). It is a more than 220 km long, NE-
485 SW seismic profile sampling the CIZ to the S of the ICS down to the boundary with the OMZ
486 (Fig. 1). Here we presented this section migrated and depth converted using a $v=6200$ m/s
487 (Figs. 2 and 7).

488 This profile presents a fairly transparent upper crust when compared to other nearby sections
489 (e.g., IBERSEIS, Fig. 8) although scarce reflectivity exists to the S coinciding with the boundary
490 (suture) between the CIZ and the OMZ, namely, the Central Unit (CU; cu in Fig. 7) and to the
491 presence of vertical folds (vf). Some very transparent zones (g) appear to be in relation with
492 the existence of granitic batholiths. To the N, the intrusion of these granites, associated to the
493 existence of normal faults (ef), is one of the evidences of extensional tectonics affecting the
494 southern part of the CIZ. The rest of the upper crust shows weak and discontinuous reflectivity
495 that responds to the existence of vertical folding affecting lithologies with little impedance

496 contrast. In fact, deformation in the upper crust of this part of the CIZ is weak, with absence of
497 low-dipping structures typical of tangential tectonics.

498 The lower crust shows a very different image to that of the upper crust. It is a thick band, of up
499 to 6 s TWT (from 4 s to 10 s), of mostly subhorizontal high amplitude reflectivity (lc) that at
500 some points appears to be cut across by N-dipping reflectors (cc). S-dipping internal reflectivity
501 is also identified although more scarce (ir). The lower crust thins in the northern end of the
502 profile, near the ICS, where intrusion of granites and other evidences of crustal re-equilibration
503 suggest that extension played a key role. Accordingly, we suggest that the mechanisms that
504 triggered this lower crustal thinning are related to melting and extension and not with
505 compression, as previously proposed (Ehsan et al., 2014; Martínez Poyatos et al., 2012), and
506 that the N dipping reflectivity observed in the top of the lower crust (c) in that area is the
507 expression of extensional tectonics.

508 One of the most striking features of this profile is the crocodile-like structure affecting the
509 lower crust at around CMP 10000 (cc and cc'). This structure, most likely related to Variscan
510 shortening, accommodates an important part of the deformation at lower crustal level and
511 evidences that sub-horizontal reflectivity of the lower crust is pre-Variscan, thus raising the
512 question about its precise age and origin. Despite the presence of this feature in the depth
513 continuation of the suture between the CIZ and the OMZ (Fig. 7a), reflectivity does not
514 crosscut the whole crust, suggesting the existence of a detachment in the top of the lower
515 crust. This contrasts with the presence in the upper crust (CU) of retro-eclogites with peak
516 metamorphic conditions of 19 kbar and ~550°C (López Sánchez-Vizcaíno et al., 2003). Finally,
517 the Moho boundary (m) is located at a fairly constant depth (~10 s TWT, i.e. 30-33 km),
518 although the lower crust seems to be preserved and a local crustal imbrication into the mantle
519 is observed underneath the crocodile-like structure. A 1D Vp profile (inset in Fig. 7d) from a
520 coincident WA-data model (Palomeras et al, in press) shows a conspicuous increase of values
521 along more than 15 km starting in the top of the lower crust (c) thus supporting its important
522 thickness.

523 **3.3.6. Central Iberia, Ossa-Morena and South Portuguese Zones (IBERSEIS section)**

524 The IBERSEIS seismic line was first presented by Simancas et al. (2003). A number of later
525 works added information and details to its interpretation (e.g., Carbonell et al., 2004;
526 Schmelzbach et al., 2007, 2008; Simancas et al., 2006). This section crosses the southernmost
527 CIZ, the whole OMZ, and most of the external SPZ (Fig. 1). It samples two major boundaries
528 interpreted as suture zones: that between the CIZ and the OMZ (CU, Azor et al., 1994) and the
529 one bounding the OMZ and the SPZ, which has been largely affected by younger Carboniferous
530 events (Pérez-Cáceres et al., 2015). The IBERSEIS profile structurally overlaps the ALCUDIA
531 profile along ~30 km, but it is displaced some 50 km to the W. A cross-section along this
532 transect together with its interpretation after migration at $v=6000$ m/s (Fig. 2) are shown in
533 figure 8.

534 This section is ~300 km long and features an outstanding reflectivity at upper and lower crustal
535 levels. In the upper crust, a wealth of N dipping reflections (t in Fig. 8) image a S verging thrust
536 and fold belt. In the SPZ, these are most reflective and probably related to normal faults
537 derived from the extension that led to the opening of the Rheic Ocean and later reactivated as

538 thrusts during the Late Carboniferous compression. Some authors link the highest reflective
539 features to the middle Carboniferous volcano-sedimentary complex (Schmelzbach et al., 2008),
540 which might have used these fractures as a conduit, thus enhancing reflectivity. In the OMZ, N
541 dipping reflections probably image Variscan thrust faults (ot) as some coincide with such
542 mapped structures. Their lesser reflectivity might indicate the lack of involvement in the
543 thrusts of lithologies that increase the impedance contrast.

544 Upper crustal reflectivity in both, the ZOM and SPZ, does not cross to the lower crust, rooting
545 at a mid-crustal level that, in the SPZ is transparent and does not have any particular
546 expression itself but does coincide with the top of the lower crust (c). However, in the OMZ, a
547 reflective layer exists at this depth (irb): it has been defined as the IBERSEIS reflective body
548 (IRB, Simancas et al., 2003), a 140 km long, high velocity conductive feature (Palomeras et al.,
549 2009) that is supposed to represent an early Carboniferous mantle-derived intrusion. Its origin
550 has been related to mantle plume activity that thinned the lithosphere and extracted mantle-
551 derived melts from the ascending asthenosphere (Carbonell et al., 2004). Its surface expression
552 are intraorogenic transtensional features (Rubio Pascual et al., 2013; Simancas et al., 2006).
553 Alternatively, Pin et al. (2008) have suggested, based on geochemical constraints, a tectonic
554 scenario of slab break-off for this feature. Internal reflectivity along the IRB is mostly
555 subhorizontal, probably due to the effect of the intrusion along a subhorizontal detachment,
556 and evidences little imprint from Variscan deformation. The body is slightly inclined to the S, at
557 odds with the detachment being the sole thrust of the OMZ upper crustal imbricates. Perhaps
558 it was, but its inclination changed during subsequent deformation, as later suggested.

559 The lower crust shows slightly different patterns in the CIZ and OMZ on one side and the SPZ
560 on the other. In the southernmost part of the CIZ and northern OMZ, N and S dipping
561 reflections define a wedge (cc) that might be the western continuation of the crocodile-like
562 structure observed in the ALCUDIA seismic line in an equivalent structural position (cc in Fig.
563 7). In this section, the limited crustal imbrication into the mantle identified in the ALCUDIA line
564 (cc' in Fig. 7) is not observed, perhaps because it only occurs further to the N or E. This
565 structure may be the reason why the IRB is shallower at this point, indicating that the latter is
566 older than the crocodile compressional feature. The rest of the lower crust shows S dipping
567 and sub-horizontal (lc) reflectivity that does not exhibit clear crosscutting relationships, thus
568 hindering their interpretation. However, near the boundary with the SPZ, this reflectivity
569 seems to be affected by N dipping features (ir) overprinting them. In the SPZ, the lower crust
570 shows a more homogeneous image, with subhorizontal reflectivity (lc) that is often cut across
571 by longer scale S dipping features (lct) that postdate them. The latter probably represent
572 fractures that firstly accommodated the extension linked to the opening of the Rheic Ocean
573 and were then reactivated as thrusts during the late Carboniferous compression and collision
574 of the SPZ basement with the OMZ. The most conspicuous of these reflections (lct') cuts the
575 IRB in its southern part and seems to offset the lower crustal upper boundary between the SPZ
576 and the OMZ. Two 1D Vp profiles derived from coincident WA-data (Palomeras et al., 2009)
577 and shown as insets in figure 8d indicate a velocity increase starting at the top of lower crust
578 (c) and along the IRB.

579 Even though the lower crust in the OMZ and SPZ shows dipping features, none of them crosses
580 to the upper crust, thus rooting at a mid-crustal level as does the upper crustal reflectivity. This
581 implies again the existence of a discontinuity (c) in the mid-crust.

582 Despite of crossing two suture zones and imaging part of a crocodile-like structure, the
583 IBERSEIS profile shows a fairly flat Moho (m) located at ~10 s TWT, the same apparent depth as
584 in the ALCUDIA line (30-33 km). Its signature is very clear underneath the SPZ and a bit blurry
585 below the IRB.

586 **4. Discussion**

587 Simancas et al. (2013) already undertook an integrated interpretation of most of the seismic
588 sections presented here focusing on, i) the accommodation of orogenic shortening at crustal
589 scale, (ii) the relationships between convergence, crustal thickening and collisional granitic
590 magmatism, and (iii) the development of the Iberian Variscan oroclines. In this paper the same
591 sections are presented, but they have been reprocessed at stack level and time migrated using
592 a Kirchhoff algorithm. In addition, two extra sections that image the alleged mid-crustal
593 discontinuity after the Alpine reactivation are taken into account. The first one is the N-S
594 ESCIN-2 NI dataset (Fig. 4), in the CZ, where this discontinuity has remained untouched during
595 late Variscan evolution but was reactivated during the Alpine Orogeny. The second one results
596 from the CIMDEF experiment, carried out in the CIZ across the ICS, where the mid-crustal
597 discontinuity has probably been affected by crustal melting during the Late-Variscan extension
598 and by later Alpine reactivation. The latter sections fill a key gap existing in Simancas et al.
599 (2013).

600 Figures 3 to 8 represent an effort to show a homogeneous seismic image of the Iberian Massif
601 crust that eased its integrated interpretation. Next, we discuss the main observed features,
602 and how they contribute to the understanding of the structure and evolution of the Iberian
603 Massif, adding constraints to the origin of the elevation of the central Iberian Peninsula. Figure
604 9 presents a simplified sketch of the crustal layers observed in the Iberian Massif. Figure 10
605 shows a compendium of the position of the mid-crustal discontinuity and the Moho depth (in
606 TWT) along the entire Iberian Massif as deduced from seismic NI data together with a map of
607 the Iberian Peninsula Moho depth (Palomeras et al., 2017) that includes the position of the
608 seismic profiles for comparison. We will refer to these figures along most of the discussion.

609 A particular feature of the SW Iberian Massif is the relevance of left-lateral shear zones
610 associated to its suture boundaries. They displaced central and northern Iberia to the NW with
611 respect to southern Iberia (Simancas et al., 2013). The seismic sections do not provide
612 constraints about this movement, as it is perpendicular to their layout. Thus, interpretations in
613 these areas must be taken with caution.

614 **4.1. The upper crust in the Iberian Massif: a depth image of outcropping geology**

615 Most of the seismic sections display a moderate to thick upper crust (4 to 8 s TWT, Fig. 9), with
616 very variable reflectivity. Reflections coincide with outcropping Variscan structures and thus, a
617 link has been established. As such, N dipping reflectivity in the SPZ and the OMZ is related to S
618 vergent folds and thrust faults mapped at the surface. W dipping reflections in the CZ are

619 related to mapped thin-skinned thrusts. The same type of reflectivity observed in the WALZ,
620 albeit reaching deeper levels and rooting in the lower crust, has been addressed to thick-
621 skinned thrust tectonics, which in the hinterland affects the pre-Paleozoic basement.
622 Particularly interesting is the upper crustal SPZ seismic image in contrast with that of the CZ,
623 both representing external zones. While in the latter thrusts are observed to root in a shallow
624 sole detachment, in the former one reflections/thrusts root in the lower crust. This feature will
625 be discussed in the next section.

626 Only a few seismic profiles feature a transparent upper crust. Lack of reflectivity has been
627 addressed to low fold data (ESCIN-1 and ESCIN-2, Figs 3 and 4), and most importantly to the
628 existence of a re-equilibrated upper crust featuring large amounts of partial melting, as shown
629 by voluminous outcropping granitoids (ESCIN-3.2 and N of ALCUDIA, Figs. 6 and 7). The
630 existence of vertical folds affecting little reflective monotonous lithologies also results in a
631 fairly transparent upper crust in most of the ALCUDIA section (Fig. 7).

632 None of the upper crustal reflections observed in the presented Iberian Massif NI seismic
633 sections cuts across the whole crust, always rooting in a sole thrust (parts of ESCIN-1 and
634 ESCIN-3.3, Figs. 3 and 5) or in the lower crust (the rest of them).

635 **4.2. The lower crust in the Iberian Massif: accommodation of shortening, extension and its** 636 **nature**

637 The Iberian Massif dataset presented here shows a very coherent image of the lower crust. Its
638 reflectivity is high and usually subhorizontal. However, cross cutting relationships with later
639 features of opposite dips evidence a multi-phase origin for this reflectivity.

640 The SPZ, OMZ, WALZ, CZ and the southern CIZ show that this part of the crust is also thick (4 to
641 6 s TWT). However, the ESCIN-3.2 and the northern part of the ALCUDIA sections (Figs. 1, 6 and
642 7) indicate that, in the northern CIZ, the lower crust is much thinner (1 to 2 s TWT) and
643 irregular (ESCIN-3.2, Figs. 6 and 9). This thin lower crust has been observed in areas
644 characterized by outcropping syn-collisional granitoids (zone II of Simancas et al., 2013). These
645 witness crustal re-equilibration processes triggered by gravitational collapse, extension and
646 crustal melting during the Late Carboniferous. The straightforward conclusion is to attribute
647 this thin lower crust to late Variscan orogenic extension, which features at the surface high
648 metamorphic offsets (chlorite to sillimanite zone, Díez Balda et al., 1995) and melting, implying
649 that crustal thinning has been accommodated at upper and lower crustal levels.

650 **4.2.1. Effects and outreach of late Variscan extension in the CIZ lower crust: CIMDEF,** 651 **ALCUDIA and ESCIN-3.2 sections**

652 The CIZ is a conflicting area. Although, a NI data gap exists in most of the northern CIZ, the
653 CIMDEF autocorrelation profiles (Figs. 1 and 9 and), based on passive source seismic data,
654 show a thick (~5 s TWT) lower crust in most of this area (Andrés et al., 2019, 2020). This is in
655 conflict with the NI sections ESCIN-3.2 and northernmost ALCUDIA, where the highly reflective
656 lower crust is less than half as thick (1-2 s TWT). However, granitoids are probably scarce in the
657 Variscan basement sampled by CIMDEF and hidden under the DB (Fig. 1), explaining the
658 prevalence of a thick lower crust. But in and near the ICS batholith, a rather continuous

659 internal reflection in the lower crust could be interpreted as its top part (Figs. 9 and 10), thus
660 indicating that crustal thinning and melting, observed in the surface, has also affected the
661 lower crust (Andrés et al., 2020).

662 Extension in the northern CIZ occurred simultaneously with shortening in the SW Iberian
663 Massif. According to Simancas et al. (2013) this suggests that the tectonic stresses would be
664 dominantly compressional, still induced by ongoing collision. In fact, gravitational instabilities
665 in a thickened crust should mostly be affecting the upper crust. In this context, theoretical
666 models (Royden, 1996; Seyferth and Henk, 2004) indicate that beneath areas of extension in
667 the upper crust, shortening may prevail in the lower crust. This mechanism is an efficient way
668 for syn-convergent exhumation of deep rocks.

669 Indeed, from a regional tectonic perspective, compression was active till the end of the
670 Variscan orogeny, and at times, clearly simultaneous with extension (C3 and E2 overlapped in
671 the interval 315-305 Ma; Martínez Catalán et al., 2014). But it is clear that extension affected
672 the lower crust, as it is thinned in areas of transparent, extended molten upper crust (ESCIN-
673 3.2 and ALCUDIA sections, Figs. 6 and 7). However, the irregular geometry of the ESCIN-3.2
674 lower crust might indicate the existence of folds in this re-equilibrated layer, witnessing the
675 simultaneity of extension and compression at lower crustal level (Fig. 6). However, we cannot
676 rule out that these undulations represent boudinage (i.e. extension) or Alpine folding,
677 although we consider the latter less likely.

678 In the ALCUDIA section, the imaged part of the CIZ underwent only moderate upper crustal
679 shortening (Martínez Poyatos et al., 2012). However, it exhibits a thick laminated lower crust
680 representing pre-Pennsylvanian (most probably pre-Variscan) ductile deformation (Simancas
681 et al., 2013). In addition, the latter appears deformed in two sectors near both ends of the
682 profile, concentrating deformation in discrete structures. The first of them is the very
683 conspicuous crocodile-like structure observed in the southern end, and also imaged in the
684 northern part of the IBERSEIS line (Fig. 9b). This structure mimics localized crustal indentation
685 of the OMZ into the CIZ, producing a local underthrusting of the latter to the S that is still
686 (partly?) preserved. Indentation generated tectonic inversion of the Los Pedroches early
687 Carboniferous basin (Simancas et al., 2013) and bending of the overlying upper crust, as seen
688 by the uplift of the IRB, both of which predate the imbrication. The Los Pedroches batholith
689 intruded above at 314-304 Ma in an extensional setting (Carracedo et al., 2009), postdating
690 the age of the wedge as no further deformation affected the batholith. This crocodile-like
691 feature probably represents early Carboniferous Variscan compressional deformation and
692 must account for part of the shortening observed at upper crustal level.

693 Contrarily, to the NE of this section, a ramp-and-flat geometry has been interpreted as a major
694 lower crustal thrust (Martínez Poyatos et al., 2012; Simancas et al., 2013) that helped to
695 compensate upper and lower crustal shortening. However, the highly reflective lower crust is
696 not repeated in the hanging wall to the structure, so that a subtractive character is a
697 reasonable alternative. As stated above, the thin lower crust to the N of the ramp seems to
698 evidence lower crustal thinning (Fig. 9b), as it underlies an area of upper crustal extension, the
699 Toledo gneiss dome, characterized by normal faulting and pervasive partial melting (Barbero,
700 1995; Hernández Enrile, 1991). Regardless of how much shortening that area accommodated

701 during crustal thickening and even though the observed ramp could be a thrust fault
702 reactivated by later extension, the present image of the lower crust does not suggests
703 compensation of upper crustal shortening. But the lower crust in the ALCUDIA section is
704 anomalously thick elsewhere (up to 6 s TWT, 18 km) suggesting the possibility of important
705 ductile thickening previous to the extension that triggered thinning at its northern part.

706 **4.2.2. Lower crust signature in SW Iberia: The IBERSEIS and southern ALCUDIA sections**

707 S of the CIZ, the IBERSEIS lower crust reflectivity is also subhorizontal but disrupted by N and S
708 dipping features (Fig. 9b). Whereas in the OMZ these features usually dip to the N, as do the
709 upper crustal reflections representing Variscan thrusts, in the SPZ they surprisingly mirror the S
710 dipping upper crustal Variscan thrusts. Furthermore, one of these features, placed close to the
711 boundary with the OMZ, affects almost the entire lower crust.

712 Orogenic orthogonal shortening in the upper crust has been estimated in 120 km (~57%) for
713 the OMZ and ~80 km (~45%) or even less for the SPZ (Pérez-Cáceres et al., 2016). According to
714 Simancas et al. (2013), the crocodile structure and a hypothetical northward subduction of the
715 OMZ might account for this shortening in the OMZ. Similarly, in the SPZ, the lower crustal
716 imbricated structures represent only ~ 20 km of shortening so that a detached lower crustal
717 subduction along the OMZ/SPZ might have accommodated the other 60 km.

718 In this regard, we suggest that the present day SPZ crustal image represents its decoupled
719 early Carboniferous extension and later compression. This evolution would have erased any
720 evidences of previous (pre-Carboniferous) subduction, and forced the SPZ to thin during
721 extension. i.e., the lower crust had to decrease its thickness ductilely, perhaps first in a more
722 or less distributed way and later through localized shear zones (brittle or not depending on the
723 depth) as it became shallower. However, the upper crust could have preserved most of its
724 original thickness, as the developing basins associated to extension would have been
725 constantly fed by sediments and igneous extrusions and intrusions (like the IRB in the OMZ).
726 Later compression would have folded and thrust the upper crust, and also thickened the
727 lower crust. A few lower crustal normal shear zones might have developed during extension
728 and then be reactivated as ductile thrusts during compression. Those are today observed as S
729 dipping reflections that disrupt the previous subhorizontal reflectivity in the lower crust and
730 mirror the upper crustal thrusts. Accordingly, distributed ductile deformation and thrusting
731 might have thickened the lower crust back to its original (or simply stable) thickness in the SPZ,
732 something that cannot be quantified but would need to be accounted for when comparing
733 shortening at upper and lower crustal levels. The resulting seismic image of the SPZ would
734 then be that of an extended and then inverted margin, with mirroring reflectors in the upper
735 and lower crust merging in a mid-crustal discontinuity and providing a seismic image different
736 to that of a typical foreland thrust and fold belt (e.g., CZ; Fig. 3). This evolution differs from
737 that of a hyperextended magma-rich margin as stretching of the upper and lower crust is not
738 coupled and faults do not cut across the crust and penetrate down into the mantle. In any
739 case, the S dipping lower crustal reflections, active during the Late Carboniferous, postdate
740 sub-horizontal reflectivity at the lower crust. It is worth mentioning here that the SPZ seismic
741 image is identical to that of the Rhenohercynian Massif in Germany (Franke et al., 1990;
742 Oncken, 1998) suggesting a similar evolution.

743 The discussion above shows that the lower crust in the Iberian Massif is thick, except when it is
744 affected by late orogenic extension. The mechanisms that produced lower crustal thickening
745 are probably related to compressional deformation, mostly ductile. Continental underthrusting
746 of the CZ underneath the WALZ (Ayarza et al., 1998, 2004) and part of the CIZ (Fig. 6, 9 and 10),
747 indentation of the OMZ in the CIZ (Figs. 9 and 10) and Variscan thrust-like structures probably
748 played an important role. In addition, the latter help to constrain the age of the subhorizontal
749 reflectivity. Frequent disruption of subhorizontal lower crustal lamination by Variscan (late
750 Carboniferous) dipping features indicates that the lamination developed prior to Variscan
751 compressional deformation. What this lamination represents is still an open question.

752 **4.2.3. Origin of the lower crust lamination**

753 Many vertical incidence seismic reflection profiles worldwide have shown reflective and
754 laminated lower crusts (e.g., Meissner et al., 2006; Wever, 1989) that have often been related
755 to late orogenic extensional events (Meissner, 1989). In the Iberian Massif, surface geology
756 shows that late orogenic extension affects the upper crust, mainly in areas of large previous
757 thickening. But in contrast to the latter author's models, important thinning of the lower crust
758 takes place in those areas (ESCIN-3.2 and northern ALCUDIA, Figs. 6, 7 and 9). Certainly, lower
759 crustal lamination might come from underplating eased by extension in magma rich margins
760 (Klemperer et al., 1986). But also, ductile deformation is a very likely source of lower crustal
761 lamination. Dipping events observed in the lower crust crosscutting a strong banded
762 reflectivity represent the latest orogeny-related shortening, which will be further flattened and
763 horizontalized in the next orogeny. Continuous superposition of deformational events at lower
764 crustal level may decrease the dip of structural/lithological markers and define a subhorizontal
765 fabric. These deformation mechanisms can generate structures with a strong anisotropy,
766 which results in laminated lower crustal fabrics (Carbonell and Smithson, 1991; Okaya et al.,
767 2004). Accordingly, a laminated lower crust may represent an overly reworked lower crust that
768 has been ductilely deformed over several orogenies. Opposite to the model by Meissner
769 (1989), such a horizontal reflectivity is observed along the Iberian Massif in areas where late
770 orogenic extension is absent or weak: the SPZ (Avalonia), the OMZ (peri-Gondwana), the not
771 extended CIZ, the WALZ and the CZ (Gondwana). Thus, we suggest that strong lamination in
772 the deep crust is probably a global characteristic of reworked lower crusts not affected by late
773 orogenic extension in the latest orogeny.

774 **4.3. The Moho and crustal thickness in the Iberian Massif**

775 The crust-mantle boundary, i.e., the Moho, is basically flat in the Iberian Massif except where
776 affected by Alpine tectonics (Fig. 10). This is rather surprising as the lower crust seems to be
777 quite well preserved, suggesting that the Moho geometry has been flattened out through
778 slow, not invasive, readjustments.

779 Flat Mohos imply the existence of either isostatic and/or thermal, late to post-orogenic
780 processes that have managed to eliminate crustal roots (Cook, 2002). NW Iberia was affected
781 by late Carboniferous extension that heated and reworked the CIZ, possibly without significant
782 mantle involvement (Alcock et al., 2009, 2011), but producing crustal thinning (Palomeras et
783 al., 2017: see Moho depth map in Fig. 10). Thick and thermally mature crusts might experience
784 lateral flow of its low-viscosity deeper part that contributes to reduce crustal roots (Seyferth

785 and Henk, 2004). This process might have partly occurred in the CIZ sampled by the ESCIN-3.2
786 section (Fig. 6) where an outstanding change in lower crustal thickness and signature exists,
787 manifested by a thinner and very reflective lower crust in contrast to that to the E, in the WALZ
788 (1 vs 3 s TWT) or to the S, in the ALCUDIA profile (1 vs 5-6 s TWT). In the former, the Variscan
789 crust is still thick even though it experienced late-Variscan extension in its western part and
790 the whole area was slightly affected by Permian and Mesozoic extension, the latter linked to
791 the opening of the Bay of Biscay. In fact, underthrusting of the CZ lower crust is still preserved
792 in the eastern CIZ (Figs. 6 and 9).

793 In the SW Iberian Massif, a thick laminated lower crust is still observable while the Moho depth
794 is fairly constant (~10s TWT). Carboniferous-to-Permian isostatic rebound in response to
795 tectonic thickening, erosion and localized Permian thermal readjustments must have
796 contributed to flatten the Moho. However, seismic reflections show that crustal imbrication
797 into the mantle has locally survived post-orogenic Moho resetting. This indicates that isostatic
798 equilibrium has been reached in a long wavelength scale, but that local features can still
799 remain if they are supported by the crustal strength and do not pose an isostatic constraint.

800 **4.4. The (missing) middle crust in the Iberian Massif (and elsewhere?)**

801 One of the highlights of this work is the lack of a layer that can be identified with a seismic
802 middle crust. But, what is the middle crust?

803 From a metamorphic point of view, the middle crust could be ascribed to the mesozone, which
804 may be correlated to the amphibolite facies whose temperature ranges between 400-500 and
805 600-800°C, the precise limits depending on the pressure (Spear, 1993). In addition, the
806 epizone, between 200-250 and 400-500°C and typically represented by the greenschist facies,
807 is also a metamorphic entity which develops during metamorphism under several kilometers
808 of anchi- and no metamorphic rocks. The depths corresponding to these temperature intervals
809 vary with the geothermal gradient. For a Barrowian gradient, typical of a continental crust
810 undergoing collision, the depths for epizone and mesozone can be estimated around 10-20
811 and 20-30 (± 5) km respectively. Although the boundaries of these metamorphic zones might
812 have a gravity, i.e. density signature, they lack a seismic one. Furthermore, epi-, meso- and
813 catazonal rocks outcrop everywhere in any eroded orogenic belt defining a very complex
814 pattern that contrasts with the simplicity of seismic images. This implies that the metamorphic
815 middle-crust does not need to coincide with a hypothetical seismic middle crust, the former
816 often being part the upper crust in ancient orogens.

817 Seismic data are sensible to velocity and density contrasts and not to the absolute value of
818 velocity and density. If a sharp contrast exists, a reflection appears, but metamorphic zones
819 usually lack sharp boundaries. So from a seismic point of view, a middle crust should be a
820 crustal level bounded in its upper and lower parts by reflections indicative of the existence of
821 important impedance contrasts at its top and bottom. In this regard, only the IRB, intruded
822 between the upper and the lower crust (Carbonell et al., 2004; Simancas et al., 2003), and
823 providing conspicuous velocity contrasts (Palomeras et al., 2009, 2011) fulfills that
824 requirement. However, it is most probably an intrusion emplaced at a mid-crustal discontinuity
825 and does not represent the middle crust.

826 WA reflection seismic data from the northern Iberian Massif have often resulted in
827 multilayered models despite weak evidences of continuous reflectivity at these levels (Ayarza
828 et al., 1998; Fernández-Viejo et al., 1998, 2000; Pedreira et al., 2003). Even though local
829 velocity contrasts capable of providing weak and patchy reflectivity exist at different crustal
830 depths (e.g., thrust faults and normal detachments may represent lithological boundaries with
831 a noticeable velocity contrast), these are not orogen-scale features but local reflectors.
832 However, many of these reflections have been extrapolated and interpreted as middle crust in
833 seismic WA datasets, despite of being part of upper crust when compared with NI data, i.e., lie
834 above the mid-crustal discontinuity (e.g., Vp increase at ~10 km in Fig. 5e). In this regard, the
835 short wavelength heterogeneities of the crust have been often considered by low resolution
836 WA datasets as laterally continuous features (Levander and Holliger, 1992), something that has
837 led us to wrong models.

838 According to the above we argue that, in the Iberian Massif, no seismic middle crust can be
839 identified. In the hinterland, reflectors imaging deformation in the upper crust root in the top
840 of the lower crust. Only in ESCIN-1, which depicts the thin-skinned deformation of the CZ,
841 thrust faults root in a sole thrust and one could argue that the basement underneath these
842 shallow reflections represents the middle crust. But in the shallower part, to the E, early
843 Paleozoic and Neoproterozoic sediments occur on both sides of the sole thrust. Also, in the
844 deeper parts, to the W, the previous crystalline basement is probably involved in imbrications
845 affecting the upper crust. Thus, in our opinion, that non-reflective basement represents the
846 seismic upper crust.

847 In the Iberian Massif, the Paleozoic was deposited unconformably above Neoproterozoic
848 sediments which could be considered as its basement, but these were not metamorphic then.
849 Only in the OMZ, greenschist to amphibolite facies Neoproterozoic represents the Cadomian
850 basement, but it cannot be distinguished from the overlying Paleozoic metasediments in the NI
851 profiles. An even older crystalline basement of felsic composition exists, as indicated by
852 inherited zircons of 830-2000 Ma found in Ediacaran orthogneisses, Lower Ordovician
853 volcanics and Variscan granitoids that resulted from partial melting of such a basement
854 (Fernández-Suárez et al., 1998; Montero et al., 2007; Villaseca et al., 2012). Again, its upper
855 boundary is not imaged on NI profiles. These data also suggest that, in the Iberian Massif,
856 there are no crustal intervals that can be related to a seismic middle crust. Decoupling of
857 reflectivity, i.e. deformation, at a mid-crustal level led us to define just an upper and a lower
858 crust.

859 **4.5. Significance of a mid-crustal discontinuity: Geometry and lateral extent**

860 Inspection of the Iberian Massif NI seismic dataset leads us to conclude that an orogenic-scale
861 mid-crustal discontinuity exists. This surface does not always provide a clear reflection, as in the
862 SPZ, but it is clearly defined by the geometry of the upper and lower crustal reflections,
863 asymptotically merging into it. The discontinuity coincides with the top of the lower crust,
864 which is often much more reflective than the upper crust and features a Vp increase.
865 Furthermore, this discontinuity has probably acted as a detachment for Variscan deformation
866 in the hinterland of the orogen and in the SPZ. However, in the CZ, the transition between

867 upper and lower crust is poorly defined, as most of its basement was not affected by Variscan
868 tectonics.

869 Simancas et al. (2013) already described this discontinuity on the basis of the asymptotic
870 geometry of the SPZ faults towards the middle of the crust. These authors concluded that its
871 depth greatly varies when reaching suture boundaries, where the discontinuity roots. Although
872 we do not observe a subduction zone in the reworked elusive suture between the SPZ and the
873 OMZ (Pérez-Cáceres et al., 2015), and interpret the OMZ/CIZ suture as an indentation between
874 two continental crusts, triggering imbrication into the mantle of the latter (crocodile
875 structure), we agree that this discontinuity would have eased the decoupling of the Iberian
876 crust, allowing subduction of its lower part while the upper part was deformed by folds and
877 thrust faults. In fact, this is clearly observed in the Alpine northward subduction of the Iberian
878 Massif lower crust underneath the CZ (ESCIN-2, Fig. 4) and also, in the Pyrenees, where a
879 detached Iberian lower crust subducts to the N (Teixell et al., 2018). But in the Iberian Massif,
880 the complexity of Variscan tectonics and late-Variscan crustal re-equilibration has mostly
881 removed evidences of a such mechanisms, although a comparable example has been
882 preserved in the NW: the thick lower crust imaged by ESCIN-3.3 is interpreted as
883 underthrusting of the CZ lower crust under that of the WALZ (Ayarza et al., 1998; Martínez
884 Catalán et al., 2003, 2012, 2014), even reaching the CIZ, as shown in profile ESCIN-3.2.

885 Some authors have interpreted the Iberian Massif mid crustal discontinuity as the brittle-
886 ductile transition (e.g. Ehsan et al., 2014; Simancas et al., 2013). Indeed, it bounds a lower
887 crust, highly reflective and ductilely deformed from the upper crust. However, Variscan ductile
888 deformation occurs also above the discontinuity in the entire Iberian Massif, with the
889 exception of the CZ. On the other side, if we deal with present deformation mechanisms, it is
890 unlikely that the brittle-ductile transition, which depends on P and T values, coincided with
891 the described discontinuity, because, i) it does not necessarily imply an impedance contrast
892 (Litak and Brown, 1989), and ii) according to figure 10, the depth of the discontinuity varies
893 from 4 s TWT (~12 km, ALCUDIA section) to 8 s TWT (~21 km, ESCIN-2 section) which would
894 imply unrealistic crustal P and T variations. Accordingly, a different interpretation must be
895 sought.

896 The Iberian laminated lower crust is probably very old. Granulites dredged in Mesozoic
897 sediments of the Cantabrian margin have yielded ages of up to 1400 Ma (Capdevila et al., 1980
898 and references therein). Even older Ar-Ar values (~2500 Ma) have been obtained for the
899 Galicia Bank granulites (Gardien et al., 2000). These granulites have been deformed ductilely
900 during several orogenies. But rocks lying above the lower crust, whatever their nature, are
901 separated from it by a discontinuity that fosters decoupled deformation between both crustal
902 layers. Accordingly, the observed mid-crustal discontinuity probably represents a rheological
903 boundary that separates rocks that have been deformed differently. This boundary, located at
904 the top of the lower crust, represents a velocity increase as the latter is probably composed of
905 dense granulites and includes relatively abundant basic rocks, which makes it easily
906 identifiable in NI and WA seismic sections.

907 The geometry of this discontinuity and its depth, together with that of the Moho (Fig. 10),
908 provide insights of the evolution of the Iberian Massif. Along the SW Iberian Massif, the mid-

909 crustal discontinuity is sub-horizontal and lies at a depth between 4-6 s TWT. In the OMZ, the
910 intrusion of the IRB allows to establish its depth in the top or the bottom of this feature, but in
911 average, its location would fit the above given values. However, in the center and NW, the
912 position of the discontinuity varies, deepening down to 8 s TWT (Figs. 9 and 10).

913 The low resolution autocorrelation models obtained along the CIMDEF profile show confusing
914 results along the central Iberian Massif. There, the mid-crustal discontinuity might lie at 5-6 s
915 TWT, deepening around the ICS to 8 s TWT as it has been affected by pervasive extension and
916 melting, thus defining a thin lower crust (2 s TWT, ~6 km, Figs. 9 and 10). Accordingly, this
917 feature appears redefined in this area, and now follows the geometry of the ICS batholith. The
918 deepening of this discontinuity and associated thinning of the lower crust might have allowed
919 coupled deformation, letting part of the upper crust to the S of the ICS to underthrust it
920 (Andrés et al., 2020). This would foster the 400-500 m topographic change between the N and
921 S foreland basins of this Alpine mountain range (Fig. 9). In fact, Simancas et al. (2013) argues
922 that coupled crustal deformation takes place when a relatively weak lower crust exists
923 something that might well represent the context of the ICS. The resulting geometry of this
924 Alpine reactivation and its topographic imprint is different to that observed to the N, in the CZ,
925 where late orogenic extension and melting does not exist and the mid-crustal discontinuity has
926 been preserved.

927 The most outstanding change in the mid-crustal discontinuity architecture appears in NW
928 Iberia, along the ESCIN-3.2 profile. This section features the thinnest crust (9 s TWT)
929 accompanied by the thinnest lower crust (~1 s TWT). The mid-crustal discontinuity lies at 8 s
930 TWT in contrast to the depth where it appears in the neighbouring ESCIN-3-3 and ESCIN-1 lines
931 (6-8 s TWT), suggesting that it has been redefined. Nevertheless, clear reflections root in its
932 upper part indicating that it still acted as a discontinuity/detachment. Accordingly, we suggest
933 that in NW Iberia, gravitational collapse followed by crustal melting and extension has thinned
934 the crust (Fig. 10), and specially the lower crust, relocating the mid-crustal discontinuity.

935 NW Iberia was importantly thickened (up to 50-70 km) due to the emplacement of the GTMZ
936 allochthonous complexes. Thermal models by Alcock et al. (2009, 2015) show that as a result,
937 the upper mantle continued increasing its temperature 60-65 Ma after the start of
938 compressional deformation at 360 Ma. This implies large thinning of the mantle lithosphere,
939 from 70 to 25-30 km, due to the ascent of the 1300 °C isotherm. It is not surprising that the
940 lower crust there became highly extended as a consequence of the heat increase, as in the
941 models it reached 800 °C after 45 Ma and 900 °C after 55 Ma (315-305 Ma).

942 **4.5.1. The Iberian Massif Conrad discontinuity**

943 The idea of a mid-crustal velocity discontinuity was put forward in the 1920's (Conrad, 1925).
944 Early analysis of natural source earthquake recordings and later images from controlled source
945 seismic reflection data provided further evidences that supported a clear distinction between
946 upper and lower crust. These evidences led to consider the Conrad discontinuity as a global
947 scale feature present in the continental crust. However, this was later challenged as some
948 results of deep seismic reflection profiling did not show a clear distinction between upper and
949 lower crust (Litak and Brown, 1989).

950 Mid-crustal discontinuities have, however, been observed often in different types of seismic
951 data worldwide (e.g., Fianco et al., 2019; Hobbs et al., 2004; Melekhova et al., 2019; Oncken,
952 1998; Ross et al., 2004; Snelson et al., 2013). Important changes in the rheology of the crust
953 have also been reported at those depths (Maggini and Caputo, 2020; Wever, 1989) supporting
954 the idea that a mechanical boundary must exist. Thus, we suggest that, even though it is not
955 observed everywhere (Litak and Brown, 1989), this feature is an orogen-scale, world class
956 continental crustal discontinuity (Artemieva, 2009), often coinciding with the top of the highly
957 laminated lower crust (when there is one). Its existence might determine the way the crust
958 deforms, easing decoupled deformation. Orogenic evolution, i.e. rifting, extension, melting,
959 etc. may modify it or even erase it, thus its existence and geometry might help us to
960 understand the geologic history of continents. In this regard, and coming back to the long-
961 forgotten discussion of the nature of the Conrad discontinuity (Conrad, 1925) and its position
962 on top of the laminated lower crust (Wever, 1989), we suggest that, in the Iberian Massif, the
963 observed mid-crustal feature fulfills the characteristics of this debated discontinuity. Its clear
964 signature and regional extension contributes to unravel its nature and significance.

965 **5. Conclusions**

966 Normal incidence seismic data acquired across the Iberian Massif in the last 30 years have
967 provided an entire image of a well exposed and almost complete part of the European
968 Variscides. Existing gaps in the central part have been recently sampled by passive source
969 seismic recordings (noise and earthquakes) that provide fairly good constraints on the crustal
970 structure.

971 Results show that crustal thickness varies from ~ 9 s TWT in late-Variscan extended areas (NW
972 of the Central Iberian Zone), to ~ 10 s TWT (30-33 km) in the external South Portuguese Zone to
973 ~ 12 s TWT (36-38 km) in the internal West Asturian-Leonese Zone. Alpine reactivation has
974 managed to further thicken the crust to at least ~ 14 s TWT (42-45 km) in the external
975 Cantabrian Zone and to 35-38 km in the Iberian Central System, a Tertiary orogenic belt
976 developed in Central Spain. The top of an often thick (up to 6 s TWT) and very reflective lower
977 crust helps to define a mid-crustal discontinuity across the entire Iberian Massif. This boundary
978 represents a level where reflections from the upper and lower crust merge asymptotically,
979 thus suggesting that it has often acted as a detachment or a decoupling level. Its position and
980 geometry varies mostly in relation to the late Variscan evolution. Accordingly, it is deeper in
981 NW and central Iberia (~ 8 s TWT), where Variscan crustal thickening was important and
982 gravitational collapse melted and extended the crust, thus defining a very thin lower crust.
983 However, it appears between 4-6 s TWT to the SW, where the crust did not thicken as much
984 and its original structure is better preserved, being later re-equilibrated through slow isostasy
985 and erosion.

986 This discontinuity exists in all the Iberian Massif tectonic zones, regardless of their Gondwana
987 or Avalonia affinity, thus suggesting it is an orogenic-scale discontinuity. We interpret it as the
988 rheological boundary between an overly ductilely deformed old lower crust and a
989 heterogeneous variably (often also ductilely) deformed upper crust that mostly (but not only)
990 shows evidences of the latest orogenic event. Its geometry, position and extent match the
991 characteristics defined for the long-forgotten Conrad discontinuity. The identification of similar

992 features in normal incidence profiles worldwide supports its inclusion as a major crustal
993 discontinuity.

994 **Acknowledgements**

995 The seismic data was reprocessed using the commercial seismic signal processing software
996 Claritas. Funding for this research was provided by the Junta de Castilla y León (SA065P17 and
997 SA084P20), the Spanish Ministry of Science and Innovation (CGL2016-78560-P) and the
998 Generalitat de Catalunya (grant 2017SGR1022). The comments of Prof. R.W.H. Butler and an
999 anonymous reviewer have greatly contributed to improve this manuscript.

1000 **References**

- 1001 Alcock, J. E., Martínez Catalán, J. R., Arenas, R. and Díez Montes, A.: Use of thermal modeling
1002 to assess the tectono-metamorphic history of the Lugo and Sanabria gneiss domes, Northwest
1003 Iberia, *Bull. la Soc. Geol. Fr.*, 180(3), 179–197, doi:10.2113/gssgfbull.180.3.179, 2009.
- 1004 Alcock, J. E., Martínez Catalán, J. R. and Arenas, R.: One- and two-dimensional models are
1005 equally effective in monitoring the crust's thermal response to advection by large-scale
1006 thrusting during orogenesis, *Comput. Geosci.*, 37(8), 1205–1207,
1007 doi:10.1016/j.cageo.2011.02.012, 2011.
- 1008 Alcock, J. E., Martínez Catalán, J. R., Rubio Pascual, F. J., Díez Montes, A., Díez Fernández, R.,
1009 Gómez Barreiro, J., Arenas, R., Dias da Silva, Í. and González Clavijo, E.: 2-D thermal modeling
1010 of HT-LP metamorphism in NW and Central Iberia: Implications for Variscan magmatism,
1011 rheology of the lithosphere and orogenic evolution, *Tectonophysics*, 657, 21–37,
1012 doi:10.1016/j.tecto.2015.05.022, 2015.
- 1013 Alonso, J. L.: Sequences of thrusts and displacement transfer in the superposed duplexes of the
1014 Esla Nappe Region (cantabrian zone, nw spain), *J. Struct. Geol.*, 9(8), 969–983,
1015 doi:10.1016/0191-8141(87)90005-8, 1987.
- 1016 Alonso, J. L., Marcos, A. and Suárez, A.: Paleogeographic inversion resulting from large out of
1017 sequence breaching thrusts: The León Fault (Cantabrian zone, NW Iberia). A new picture of the
1018 external Variscan thrust belt in the Ibero-Armorican arc, *Geol. Acta*, 7(4), 451–473,
1019 doi:10.1344/105.000001449, 2009.
- 1020 Álvarez-Marrón, J., Pérez-Estaún, A., Dañobeitia, J. J., Pulgar, J. A., Martínez Catalán, J. R.,
1021 Marcos, A., Bastida, F., Ayarza, P., Aller, J., Gallart, A., González-Lodeiro, F., Banda, E., Comas,
1022 M. C. and Córdoba, D.: Seismic structure of the northern continental margin of Spain from
1023 ESCIN deep seismic profiles, *Tectonophysics*, 264, 153–174, doi:10.1016/S0040-
1024 1951(96)00124-2, 1996.
- 1025 Andrés, J., Draganov, D., Schimmel, M., Ayarza, P., Palomeras, I., Ruiz, M. and Carbonell, R.:
1026 Lithospheric image of the Central Iberian Zone (Iberian Massif) using global-phase seismic
1027 interferometry, *Solid Earth*, 10(6), 1937–1950, doi:10.5194/se-10-1937-2019, 2019.
- 1028 Andrés, J., Ayarza, P., Schimmel, M., Palomeras, I., Ruiz, M. and Carbonell, R.: What can seismic
1029 noise tell us about the Alpine reactivation of the Iberian Massif? An example in the Iberian
1030 Central System, *Solid Earth*, 11(6), 2499–2513, doi:10.5194/se-11-2499-2020, 2020.
- 1031 Arenas, R., Farias, P., Gallastegui, G., Gil Ibarguchi, I., González Lodeiro, F., Klein, E., Marquínez,
1032 J., Martín Parra, L. M., Martínez Catalán, J. R., Ortega, E., de Pablo Maciá, J. G., Peinado, M. and

- 1033 Rodriguez Fernández, L. R.: Características geológicas y significado de los dominios que
1034 componen la Zona de Galicia-Trás-os- Montes. Simposio sobre Cinturones Orogénicos, in
1035 Simposio sobre Cinturones Orogénicos. II congreso Geológico de España, pp. 75–84, SGE., 1988.
- 1036 Arenas, R., Martínez Catalán, J. R., Martínez Sánchez, S., Díaz García, F., Abati, J., Fernández-
1037 Suárez, J., Andonaegui, P. and Gómez-Barreiro, J.: Paleozoic ophiolites in the Variscan suture of
1038 Galicia (northwest Spain): Distribution, characteristics, and meaning, *Mem. Geol. Soc. Am.*,
1039 200(22), 425–444, doi:10.1130/2007.1200(22), 2007.
- 1040 Artemieva, I.: Continental Crust, Geophysics and Geochemistry Vol.II -Encyclopedia of Earth
1041 and Atmospheric Sciences in the Global Encyclopedia of Life Support Systems, UNESCO., 2009.
- 1042 Ayarza, P., Martínez Catalán, J. R., Gallart, J., Pulgar, J. A. and Dañobeitia, J. J.: Estudio Sismico
1043 de la Corteza Ibérica Norte 3 . 3 : A seismic image of the Variscan crust inthe hinterland of the
1044 NW Iberian Massif, *Tectonics*, 17(2), 171–186, 1998.
- 1045 Ayarza, P., Martínez Catalán, J. R., Alvarez-Marrón, J., Zeyen, H. and Juhlin, C.: Geophysical
1046 constraints on the deep structure of a limited ocean-continent subduction zone at the North
1047 Iberian Margin, *Tectonics*, 23(1), doi:10.1029/2002TC001487, 2004.
- 1048 Azor, A., Lodeiro, F. G. and Simancas, J. F.: Tectonic evolution of the boundary between the
1049 Central Iberian and Ossa-Morena zones (Variscan belt, southwest Spain), *Tectonics*, 13(1), 45–
1050 61, doi:10.1029/93TC02724, 1994.
- 1051 Azor, A., Rubatto, D., Simancas, J. F., González Lodeiro, F., Martínez Poyatos, D., Martin Parra,
1052 L. M. and Matas, J.: Rhenic Ocean ophiolitic remnants in southern Iberia questioned by SHRIMP
1053 U-Pb zircon ages on the Beja-Acebuches amphibolites, *Tectonics*, 27(5), 1–11,
1054 doi:10.1029/2008TC002306, 2008.
- 1055 Bandrés, A., Eguíluz, L., Pin, C., Paquette, J. L., Ordóñez, B., Le Fèvre, B., Ortega, L. A. and Gil
1056 Ibarra, J. I.: The northern Ossa-Morena Cadomian batholith (Iberian Massif): Magmatic arc
1057 origin and early evolution, *Int. J. Earth Sci.*, 93(5), 860–885, doi:10.1007/s00531-004-0423-6,
1058 2004.
- 1059 Barbero, L.: Granulite-facies metamorphism in the Anatectic Complex of Toledo, Spain: late
1060 Hercynian tectonic evolution by crustal extension, *J. Geol. Soc. London*, 152(2), 365–382,
1061 doi:10.1144/gsjgs.152.2.0365, 1995.
- 1062 BIRPS, B. I. R. P. S. and ECORS, E. de la C. C. et O. par R. et R. S.: Deep seismic reflection
1063 profiling between England, France and Ireland., *J. - Geol. Soc.*, 143(1), 45–52,
1064 doi:10.1144/gsjgs.143.1.0045, 1986.
- 1065 Bortfeld, R. K.: First results and preliminary interpretation of deep- reflection seismic
1066 recordings along profile DEKORP 2-South (FRG)., *J. Geophys. - Zeitschrift fur Geophys.*, 57(3),
1067 137–163, 1985.
- 1068 Braid, J. A., Brendan Murphy, J., Quesada, C. and Mortensen, J.: Tectonic escape of a crustal
1069 fragment during the closure of the Rhenic Ocean: U-Pb detrital zircon data from the late
1070 Palaeozoic Pulo do Lobo and South Portuguese zones, Southern Iberia, *J. Geol. Soc. London.*,
1071 168(2), 383–392, doi:10.1144/0016-76492010-104, 2011.
- 1072 Braid, J. A., Murphy, J. B., Quesada, C., Bickerton, L. and Mortensen, J. K.: Probing the
1073 composition of unexposed basement, South Portuguese Zone, southern Iberia: Implications for
1074 the connections between the Appalachian and Variscan orogens, *Can. J. Earth Sci.*, 49(4), 591–
1075 613, doi:10.1139/E11-071, 2012.

- 1076 Butler, R. W. H. and Mazzoli, S.: Styles of continental contraction: A review and introduction,
1077 Spec. Pap. Geol. Soc. Am., 414(414), 1–10, doi:10.1130/2006.2414(01), 2006.
- 1078 Capdevila, R., Boillot, G., Lepvrier, C., Malod, J. A. and Mascle, G.: Les formations cristallines du
1079 Banc Le Danois (marge nord-ibérique), CR Acad. Sci. Paris, D, 291(January), 317–320 [online]
1080 Available from:
1081 [http://scholar.google.com/scholar?hl=en&btnG=Search&q=intitle:Les+formations+cristallines+du+Banc+Le+Danois+\(marge+nord+ibérique\)#0](http://scholar.google.com/scholar?hl=en&btnG=Search&q=intitle:Les+formations+cristallines+du+Banc+Le+Danois+(marge+nord+ibérique)#0), 1980.
1082
- 1083 Carbonell, R. and Smithson, S. B.: Large-scale anisotropy within the crust in the Basin and
1084 Range province, *Geology*, 19(July), 698–701, doi:doi:10.1130/0091-7613(1991)019, 1991.
- 1085 Carbonell, R., Simancas, J. F., Juhlin, C., Pous, J., Pérez-Estaún, A., Gonzalez-Lodeiro, F., Munoz,
1086 G., Heise, W. and Ayarza, P.: Geophysical evidence of a mantle derived intrusion in SW Iberia,
1087 *Geophys. Res. Lett.*, 31(11), 1–4, 2004.
- 1088 Carracedo, M., Paquette, J. L., Alonso Olazabal, A., Santos Zalduegui, J. F., de García de
1089 Madinabeitia, S., Tiepolo, M. and Gil Iburguchi, J. I.: U-Pb dating of granodiorite and granite
1090 units of the Los Pedroches batholith. Implications for geodynamic models of the southern
1091 Central Iberian Zone (Iberian Massif), *Int. J. Earth Sci.*, 98(7), 1609–1624, doi:10.1007/s00531-
1092 008-0317-0, 2009.
- 1093 Carvalho, D.: The metallogenetic consequences of plate tectonics and the upper Paleozoic
1094 evolution of southern Portugal, *Estud. Notas e Trab. S.F.M.*, 20(3–4), 297–320, 1972.
- 1095 Casquet, C., Galindo, C., Tornos, F., Velasco, F. and Canales, A.: The Aguablanca Cu-Ni ore
1096 deposit (Extremadura, Spain), a case of synorogenic orthomagmatic mineralization: Age and
1097 isotope composition of magmas (Sr, Nd) and ore (S), *Ore Geol. Rev.*, 18(3–4), 237–250,
1098 doi:10.1016/S0169-1368(01)00033-6, 2001.
- 1099 Chopra, S. and Alexeev, V.: Application of texture attribute analysis to 3D seismic data, *Soc.*
1100 *Explor. Geophys. - 75th SEG Int. Expo. Annu. Meet. SEG 2005*, 30(7), 767–770,
1101 doi:10.1190/1.2144439, 2005.
- 1102 Conrad, V.: Laufzeitkurven des Tauernbens vom 28, *Mitt. Erdb. Komm. Wlen Akad. Wiss.*, 59, 1,
1103 1925.
- 1104 Cook, F. A.: Fine structure of the continental reflection Moho, *Bull. Geol. Soc. Am.*, 114(1), 64–
1105 79, doi:10.1130/0016-7606(2002)114<0064:FSOTCR>2.0.CO;2, 2002.
- 1106 Corretgé, L. G. and Suárez, O.: Cantabrian and Palentian Zones. Igneous Rocks, in *Pre-Mesozoic
1107 Geology of Iberia*, edited by R. D. Dallmeyer and E. Martínez García, pp. 72–79, Springer-
1108 Verlag, Berlin., 1990.
- 1109 Dallmeyer, R. D. and Quesada, C.: Cadomian vs. Variscan evolution of the Ossa-Morena zone
1110 (SW Iberia): field and $^{40}\text{Ar}/^{39}\text{Ar}$ mineral age constraints, *Tectonophysics*, 216(3–4), 339–364,
1111 doi:10.1016/0040-1951(92)90405-U, 1992.
- 1112 Dallmeyer, R. D., Martínez Catalán, J. R., Arenas, R., Gil Iburguchi, J. I., Gutiérrez-Alonso, G.,
1113 Fariás, P., Bastida, F. and Aller, J.: Diachronous Variscan tectonothermal activity in the NW
1114 Iberian Massif: Evidence from $^{40}\text{Ar}/^{39}\text{Ar}$ dating of regional fabrics, *Tectonophysics*, 277(4),
1115 307–337, doi:10.1016/S0040-1951(97)00035-8, 1997.
- 1116 DeFelipe, I., Pedreira, D., Pulgar, J. A., van der Beek, P. A., Bernet, M. and Pik, R.: Unraveling
1117 the Mesozoic and Cenozoic Tectonothermal Evolution of the Eastern Basque-Cantabrian Zone–

- 1118 Western Pyrenees by Low-Temperature Thermochronology, *Tectonics*, 38(9), 3436–3461,
1119 doi:10.1029/2019TC005532, 2019.
- 1120 DeFelipe, I., Alcalde, J., Ivandic, M., Martí, D., Ruiz, M., Marzán, I., Diaz, J., Ayarza, P.,
1121 Palomeras, I., Fernandez-Turiel, J. L., Molina, C., Bernal, I., Brown, L., Roberts, R. and Carbonell,
1122 R.: Reassessing the lithosphere: SeisDARE, an open access seismic data repository, *Earth Syst.*
1123 *Sci. Data Discuss.*, (September), 1–32, doi:10.5194/essd-2020-208, 2020.
- 1124 DEKORP Research Group: Results of deep reflection seismic profiling in the Oberpfalz (Bavaria),
1125 *Geophys. J. R. Astron. Soc.*, 89(1), 353–360, doi:10.1111/j.1365-246X.1987.tb04430.x, 1987.
- 1126 Dias, R. and Ribeiro, A.: The Ibero-Armorican Arc: A collision effect against an irregular
1127 continent?, *Tectonophysics*, 246(1–3), 113–128, doi:10.1016/0040-1951(94)00253-6, 1995.
- 1128 Díaz Azpiroz, M., Fernández, C., Castro, A. and El-Biad, M.: Tectonometamorphic evolution of
1129 the Aracena metamorphic belt (SW Spain) resulting from ridge-trench interaction during
1130 Variscan plate convergence, *Tectonics*, 25(1), 1–20, doi:10.1029/2004TC001742, 2006.
- 1131 Díez-Montes, A., Martínez Catalán, J. R. and Bellido Mulas, F.: Role of the Olló de Sapo massive
1132 felsic volcanism of NW Iberia in the Early Ordovician dynamics of northern Gondwana,
1133 *Gondwana Res.*, 17(2–3), 363–376, doi:10.1016/j.gr.2009.09.001, 2010.
- 1134 Díez Balda, M. A., Martínez Catalán, J. R. and Ayarza, P.: Syn-collisional extensional collapse
1135 parallel to the orogenic trend in a domain of steep tectonics: the Salamanca Detachment Zone
1136 (Central Iberian Zone, Spain), *J. Struct. Geol.*, 17(2), 163–182, doi:10.1016/0191-
1137 8141(94)E0042-W, 1995.
- 1138 Díez Montes, A., Martínez Catalán, J. R. and Bellido Mulas, F.: Role of the Olló de Sapo massive
1139 felsic volcanism of NW Iberia in the Early Ordovician dynamics of northern Gondwana,
1140 *Gondwana Res.*, 17(2–3), 363–376, doi:10.1016/j.gr.2009.09.001, 2010.
- 1141 Ehsan, S. A., Carbonell, R., Ayarza, P., Martí, D., Pérez-Estaún, A., Martínez-Poyatos, D. J.,
1142 Simancas, J. F., Azor, A. and Mansilla, L.: Crustal deformation styles along the reprocessed deep
1143 seismic reflection transect of the Central Iberian Zone (Iberian Peninsula), *Tectonophysics*, 621,
1144 159–174, doi:10.1016/j.tecto.2014.02.014, 2014.
- 1145 Ehsan, S. A., Carbonell, R., Ayarza, P., Martí, D., Martínez Poyatos, D., Simancas, J. F., Azor, A.,
1146 Ayala, C., Torné, M. and Pérez-Estaún, A.: Lithospheric velocity model across the Southern
1147 Central Iberian Zone (Variscan Iberian Massif): The ALCUDIA wide-angle seismic reflection
1148 transect, *Tectonics*, 34(3), 535–554, doi:10.1002/2014TC003661, 2015.
- 1149 Expósito, I., Simancas, J. F. and Lodeiro, F. G.: Estructura de la mitad septentrional de la zona
1150 de Ossa-Morena: Deformación en el bloque inferior de un cabalgamiento cortical de evolución
1151 compleja: Deformación en el bloque inferior de un cabalgamiento cortical de evolución
1152 compleja, *Rev. la Soc. Geológica España*, 15(1), 3–14, 2002.
- 1153 Expósito, I., Simancas, J. F., González Lodeiro, F., Bea, F., Montero, P. and Salman, K.:
1154 Metamorphic and deformational imprint of Cambrian - Lower Ordovician rifting in the Ossa-
1155 Morena Zone (Iberian Massif, Spain), *J. Struct. Geol.*, 25(12), 2077–2087, doi:10.1016/S0191-
1156 8141(03)00075-0, 2003.
- 1157 Farias, P., Gallastegui, G., González Lodeiro, F., Marquinez, J., Martín-Parra, L. M., Martínez
1158 Catalán, J. R. and Pablo-Maciá, J. G.: “Aportaciones al conocimiento de la litoestratigrafía y
1159 estructura de Galicia Central,” *Memórias da Fac. Ciências, Univ. do Porto*, 1(January 1987),
1160 411–431, 1987.

- 1161 Fernández-Suárez, J., Gutiérrez-Alonso, G., Jenner, G. A. and Jackson, S. E.: Geochronology and
1162 geochemistry of the Pola de Allande granitoids (northern Spain): their bearing on the
1163 Cadomian-Avalonian evolution of northwest Iberia, *Can. J. Earth Sci.*, 35(12), 1439–1453,
1164 doi:10.1139/cjes-35-12-1439, 1998.
- 1165 Fernández-Viejo, G., Gallart, J., Pulgar, J. A., Gallastegui, J., Dañobeitia, D. and Córdoba, D.:
1166 Crustal transition between continental and oceanic domains along the North Iberian margin
1167 from wide angle seismic and gravity data, *Geophys. Res. Lett.*, 25(23), 4249–4252, 1998.
- 1168 Fernández-Viejo, G., Gallart, J., Pulgar, A., Córdoba, D. and Dañobeitia, J. J.: Seismic signature
1169 of Variscan and Alpine tectonics in NW Iberia: Crustal structure of the Cantabrian Mountains
1170 and Duero Basin, *J. Geophys. Res.*, 105(1999), 3001–3018, 2000.
- 1171 Fianco, C. B., França, G. S., Albuquerque, D. F., Vilar, C. da S. and Argollo, R. M.: Using the
1172 receiver function for studying earth deep structure in the Southern Borborema Province, *J.*
1173 *South Am. Earth Sci.*, 94(April), 102221, doi:10.1016/j.jsames.2019.102221, 2019.
- 1174 Finlayson, D. M., Collins, C. D. N. and Lock, J.: P-wave velocity features of the lithosphere under
1175 the Eromanga Basin, Eastern Australia, including a prominent MID-crustal (Conrad?)
1176 discontinuity, *Tectonophysics*, 101(3–4), 267–291, doi:10.1016/0040-1951(84)90117-3, 1984.
- 1177 Flecha, I., Palomeras, I., Carbonell, R., Simancas, J. F., Ayarza, P., Matas, J., González-Lodeiro, F.
1178 and Pérez-Estaún, A.: Seismic imaging and modelling of the lithosphere of SW-Iberia,
1179 *Tectonophysics*, 472(1–4), 148–157, doi:10.1016/j.tecto.2008.05.033, 2009.
- 1180 Franke, W.: The mid-European segment of the Variscides: Tectonostratigraphic units, terrane
1181 boundaries and plate tectonic evolution, *Geol. Soc. Spec. Publ.*, 179, 35–56,
1182 doi:10.1144/GSL.SP.2000.179.01.05, 2000.
- 1183 Franke, W., Bortfeld, R. K., Brix, M., Drozdowski, G., Dürbaum, H. J., Giese, P., Janoth, W.,
1184 Jödicke, H., Reichert, C., Scherp, A., Schmoll, J., Thomas, R., Thünker, M., Weber, K., Wiesner,
1185 M. G. and Wong, H. K.: Crustal structure of the Rhenish Massif: results of deep seismic
1186 reflection lines Dekorp 2-North and 2-North-Q, *Geol. Rundschau*, 79(3), 523–566,
1187 doi:10.1007/BF01879201, 1990.
- 1188 Gallastegui, J., Pulgar, J. A. and Alvarez-Marrón, J.: 2-D seismic modeling of the Variscan
1189 foreland thrust and fold belt crust in NW Spain from ESCIN-1 deep seismic reflection data,
1190 *Tectonophysics*, 269(1–2), 21–32, doi:10.1016/S0040-1951(96)00166-7, 1997.
- 1191 Gallastegui, J., Pulgar, J. A. and Gallart, J.: Alpine tectonic wedging and crustal delamination in
1192 the Cantabrian Mountains (NW Spain), *Solid Earth*, 7(4), 1043–1057, doi:10.5194/se-7-1043-
1193 2016, 2016.
- 1194 García Casquero, J. L., Boelrijk, N. A. I. M., Chacón, J. and Priem, H. N. A.: Rb-Sr evidence for the
1195 presence of Ordovician gsrnites in the deformed basement of the Badajoz-Córdoba belt, SW
1196 Spain, *Geol. Rundschau*, 74(2), 379–384, doi:10.1007/BF01824904, 1985.
- 1197 Gardien, V., Arnaud, N. and Desmurs, L.: Petrology and ar-ar dating of granulites from the
1198 Galicia bank (Spain): African craton relics in western Europe, *Geodin. Acta*, 13(2–3), 103–117,
1199 doi:10.1080/09853111.2000.11105367, 2000.
- 1200 Gómez-Pugnaire, M. T., Azor, A., Fernández-Soler, J. M. and López Sánchez-Vizcaíno, V.: The
1201 amphibolites from the Ossa-Morena/Central Iberian Variscan suture (Southwestern Iberian
1202 Massif): Geochemistry and tectonic interpretation, *Lithos*, 68(1–2), 23–42, doi:10.1016/S0024-
1203 4937(03)00018-5, 2003.

- 1204 Gómez Barreiro, J., Martínez Catalán, J. R., Arenas, R., Castiñeiras, P., Abati, J., Díaz García, F.
 1205 and Wijbrans, J. R.: Tectonic evolution of the upper allochthon of the Órdenes complex (
 1206 northwestern Iberian Massif): Structural constraints to a polyorogenic peri-Gondwanan
 1207 terrane, *Geol. Soc. Am. Spec. Pap.*, 423, 315–332, doi:10.1130/2007.2423(15)., 2007.
- 1208 Hernández Enrile, J. L.: Extensional tectonics of the toledo ductile-brittle shear zone, central
 1209 Iberian Massif, *Tectonophysics*, 191(3–4), 311–324, doi:10.1016/0040-1951(91)90064-Y, 1991.
- 1210 Hobbs, B. E., Ord, A., Regenauer-Lieb, K. and Drummond, B.: Fluid reservoirs in the crust and
 1211 mechanical coupling between the upper and lower crust, *Earth, Planets Sp.*, 56(12), 1151–
 1212 1161, doi:10.1186/BF03353334, 2004.
- 1213 Julivert, M., Fontboté, M., Ribeiro, A. and Conde, L. E.: Mapa tectónico de la Península Ibérica
 1214 y Baleares Notas Incluye mapa : Unidades estructurales de la Península Ibérica . Escala 1 :
 1215 1.000.000., Instituto Geológico y Minero de España., 1972.
- 1216 Klemperer, S. L., Hauge, T. A., Hauser, E. C., Oliver, J. E. and Potter, C. J.: The Moho in the
 1217 northern Basin and Range Province, Nevada, along the COCORP 40oN seismic- reflection
 1218 transect. (USA)., *Geol. Soc. Am. Bull.*, 97(5), 603–618, doi:10.1130/0016-
 1219 7606(1986)97<603:TMITNB>2.0.CO;2, 1986.
- 1220 Kossmat, F.: Gliederung des varistischen Gebirgsbaues. Abhandlungen des Sächsischen, in
 1221 Abhandlungen des Sächsischen Geologuschen Landesamts, edited by A. des S. G. Landesamts,
 1222 p. 39, Leipzig, Heft 1., 1927.
- 1223 Levander, A. R. and Holliger, K.: Small-scale heterogeneity and large-scale velocity structure of
 1224 the continental crust, *J. Geophys. Res.*, 97(B6), 8797–8804, doi:10.1029/92JB00659, 1992.
- 1225 Linnemann, U., Pereira, M. F., Jeffries, T. E., Drost, K. and Gerdes, A.: The Cadomian Orogeny
 1226 and the opening of the Rheic Ocean: The diacrony of geotectonic processes constrained by LA-
 1227 ICP-MS U-Pb zircon dating (Ossa-Morena and Saxo-Thuringian Zones, Iberian and Bohemian
 1228 Massifs), *Tectonophysics*, 461(1–4), 21–43, doi:10.1016/j.tecto.2008.05.002, 2008.
- 1229 Litak, R. K. and Brown, L. D.: A modern perspective on the Conrad Discontinuity, *Eos, Trans.*
 1230 *Am. Geophys. Union*, 70(29), 713–725, doi:10.1029/89EO00223, 1989.
- 1231 López Sánchez-Vizcaíno, V., Gómez-Pugnaire, M. T., Azor, A. and Fernández-Soler, J. M.: Phase
 1232 diagram sections applied to amphibolites: A case study from the Ossa-Morena/Central Iberian
 1233 Variscan suture (Southwestern Iberian Massif), *Lithos*, 68(1–2), 1–21, doi:10.1016/S0024-
 1234 4937(03)00017-3, 2003.
- 1235 Lotze, F.: Stratigraphie und Tektonik des Keltiberischen Grundgebirges (Spanien),
 1236 Abhandlungen Gesellschaft der Wissenschaften zu Göttingen, Math. (Abh. Ges. Wiss.
 1237 Göttingen, Math.-Phys.), 14(2), 143–162, 1929.
- 1238 Maggini, M. and Caputo, R.: Sensitivity analysis for crustal rheological profiles: Examples from
 1239 the Aegean region, *Ann. Geophys.*, 63(3), 1–29, doi:10.4401/ag-8244, 2020.
- 1240 Martínez Catalán, J. R.: Are the oroclines of the Variscan belt related to late Variscan strike-slip
 1241 tectonics?, *Terra Nov.*, 23(4), 241–247, doi:10.1111/j.1365-3121.2011.01005.x, 2011.
- 1242 Martínez Catalán, J. R.: The Central Iberian arc, an orocline centered in the Iberian Massif and
 1243 some implications for the Variscan belt, *Int. J. Earth Sci.*, 101(5), 1299–1314,
 1244 doi:10.1007/s00531-011-0715-6, 2012.

- 1245 Martínez Catalán, J. R., Ayarza, P., Pulgar, J. A., Pérez-Estaún, A., Gallart, J., Marcos, A., Bastida,
1246 F., Álvarez-Marrón, J., González Lodeiro, F., Aller, J., Dañobeitia, J. J., Banda, E., Córdoba, D.
1247 and Comas, M. C.: Results from the ESCIN-N3.3 marine deep seismic profile along the
1248 Cantabrian continental margin, *Rev. Soc. Geol. España*, 8(4), 341-354., 1995.
- 1249 Martínez Catalán, J. R., Fernández-Suárez, J., Jenner, G. A., Belousova, E. and Díez Montes, A.:
1250 Provenance constraints from detrital zircon U–Pb ages in the NW Iberian Massif: implications
1251 for Palaeozoic plate configuration and Variscan evolution, *J. Geol. Soc. London.*, 161(3), 463–
1252 476, doi:10.1144/0016-764903-054, 2004.
- 1253 Martínez Catalán, J. R., Arenas, R., Diágarcía, F., González Cuadra, P., Gómez-Barreiro, J., Abati,
1254 J., Castiñeiras, P., Fernández-Suárez, J., Sánchez Martínez, S., Andonaegui, P., González Clavijo,
1255 E., Díez Montes, A., Rubio Pascual, F. J. and Valle Aguado, B.: Space and time in the tectonic
1256 evolution of the northwestern Iberian Massif: Implications for the Variscan belt, *Mem. Geol.*
1257 *Soc. Am.*, 200(21), 403–423, doi:10.1130/2007.1200(21), 2007.
- 1258 Martínez Catalán, J. R., Álvarez Lobato, F., Pinto, V., Gómez Barreiro, J., Ayarza, P., Villalaín, J. J.
1259 and Casas, A.: Gravity and magnetic anomalies in the allochthonous rdenes Complex (Variscan
1260 belt, northwest Spain): Assessing its internal structure and thickness, *Tectonics*, 31(5), 1–18,
1261 doi:10.1029/2011TC003093, 2012.
- 1262 Martínez Catalán, J. R., Rubio Pascual, F. J., Díez Montes, A., Díez Fernández, R., Gómez
1263 Barreiro, J., Dias da Silva, Í., González Clavijo, E., Ayarza, P. and Alcock, J. E.: The late Variscan
1264 HT/LP metamorphic event in NW and Central Iberia: relationships to crustal thickening,
1265 extension, orocline development and crustal evolution, *Geol. Soc. London, Spec. Publ.*, 405(1),
1266 225–247, doi:10.1144/SP405.1, 2014.
- 1267 Martínez Catalán, J. R., Díez Balda, M. A., Escuder Viruete, J., Villar Alonso, P., Ayarza, P.,
1268 Gonzalez Clavijo, E. and Díez Montes, A.: Cizallamientos dúctiles de escala regional en la
1269 provincia de Salamanca, in *Geo-Guías: Rutas Geológicas por la Península Ibérica, Canarias,*
1270 *Sicilia y Marruecos*, edited by M. Diaz Azpiroz, I. Exposito Ramos, S. Llana Fúnez, and B. Bauluz
1271 Lázaro, pp. 109–118, *Sociedad Geológica de España.*, 2019.
- 1272 Martínez García, A.: Seismic characterization and geodynamic significane of the mid-crustal
1273 discontinuity across the Variscan Iberia, *Universidad de Barcelona.*, 2019.
- 1274 Martínez García, E.: El Paleozoico de la Zona Cantabrica Oriental (Noroeste de España), *Trab.*
1275 *Geol.*, 11, 95–127, 1981.
- 1276 Martínez Poyatos, D., Carbonell, R., Palomeras, I., Simancas, J. F., Ayarza, P., Martí, D., Azor, A.,
1277 Jabaloy, A., González Cuadra, P., Tejero, R., Martín Parra, L. M., Matas, J., González Lodeiro, F.,
1278 Pérez-Estaún, A., García Lobón, J. L. and Mansilla, L.: Imaging the crustal structure of the
1279 Central Iberian Zone (Variscan Belt): The ALCUDIA deep seismic reflection transect, *Tectonics*,
1280 31(3), 1–21, doi:10.1029/2011TC002995, 2012.
- 1281 Martínez Poyatos, D. J.: Estructura del borde meridional de la Zona Centroibérica y su relación
1282 con el contacto entre las Zonas Centroibérica y de Ossa-Morena, in *Serie Nova Terra*, 18,
1283 edited by L. X. de Laxe, p. 295, *Instituto Universitario de Xeoloxía, A Coruña, Spain.*, 2002.
- 1284 Matte, P.: The Variscan collage and orogeny (480–290 Ma) and the tectonic definition of the
1285 Armorica microplate: a review - Matte - 2003 - *Terra Nova* - Wiley Online Library, *Terra Nov.*,
1286 13(1997), 122–128 [online] Available from: <http://onlinelibrary.wiley.com/doi/10.1046/j.1365-3121.2001.00327.x/full%5Cnpapers2://publication/uuid/85445613-EAD8-49D7-AE4E-704E3D282C36>, 2001.

- 1289 Matte, P. and Ribeiro, A.: Forme et orientation de l'ellipsoïde de déformation dans la virgation
1290 hercynienne de Galice. Relations avec le plissement et hypothèses sur la genèse de l'arc ibéro-
1291 armoricain, *Comptes Rendus l'Académie des Sci.*, 280, 2825–2828, 1975.
- 1292 Meissner, R.: Rupture, creep, lamellae and crocodiles: happenings in the continental crust,
1293 *Terra Nov.*, 1(1), 17–28, doi:10.1111/j.1365-3121.1989.tb00321.x, 1989.
- 1294 Meissner, R., Rabbel, W. and Kern, H.: Seismic lamination and anisotropy of the lower
1295 continental crust, *Tectonophysics*, 416(1–2), 81–99, doi:10.1016/j.tecto.2005.11.013, 2006.
- 1296 Melekhova, E., Schlaphorst, D., Blundy, J., Kendall, J. M., Connolly, C., McCarthy, A. and
1297 Arculus, R.: Lateral variation in crustal structure along the Lesser Antilles arc from petrology of
1298 crustal xenoliths and seismic receiver functions, *Earth Planet. Sci. Lett.*, 516, 12–24,
1299 doi:10.1016/j.epsl.2019.03.030, 2019.
- 1300 Montero, P., Bea, F., González-Lodeiro, F., Talavera, C. and Whitehouse, M. J.: Zircon ages of
1301 the metavolcanic rocks and metagranites of the Ollo de Sapo Domain in central Spain:
1302 Implications for the Neoproterozoic to Early Palaeozoic evolution of Iberia, *Geol. Mag.*, 144(6),
1303 963–976, doi:10.1017/S0016756807003858, 2007.
- 1304 Ochsner, A.: U-Pb geochronology of the Upper Proterozoic-Lower Paleozoic geodynamic
1305 evolution in the Ossa-Morena Zone (SW Iberia): constraints on the timing of the Cadomian
1306 orogeny, University of Zurich, Diss. ETH10, 192., 1993.
- 1307 Okaya, D., Rabbel, W., Beilecke, T. and Hasenclever, J.: P wave material anisotropy of a
1308 tectono-metamorphic terrane: An active source seismic experiment at the KTB super-deep drill
1309 hole, southeast Germany, *Geophys. Res. Lett.*, 31(24), 1–4, doi:10.1029/2004GL020855, 2004.
- 1310 Oliveira, J. T.: Part VI: South Portuguese Zone, stratigraphy and synsedimentary tectonism, in
1311 *Pre-Mesozoic Geology of Iberia*, edited by E. Dallmeyer, R. D., and Martínez García, pp. 334–
1312 347, Springer, Berlin, Germany., 1990.
- 1313 Oncken, O.: Orogenic mass transfer and reflection seismic patterns - Evidence from DEKORP
1314 sections across the European variscides (central Germany), *Tectonophysics*, 286(1–4), 47–61,
1315 doi:10.1016/S0040-1951(97)00254-0, 1998.
- 1316 Palomeras, I., Carbonell, R., Flecha, I., Simancas, J. F., Ayarza, P., Matas, J., Poyatos, D. M.,
1317 Azor, A., Lodeiro, F. G. and Pérez-Estaún, A.: Nature of the lithosphere across the Variscan
1318 orogen of SW Iberia: Dense wide-angle seismic reflection data, *J. Geophys. Res. Solid Earth*,
1319 114(2), 1–29, 2009.
- 1320 Palomeras, I., Carbonell, R., Ayarza, P., Martí, D., Brown, D. and Simancas, J. F.: Shear wave
1321 modeling and Poisson's ratio in the Variscan Belt of SW Iberia, *Geochemistry, Geophys.*
1322 *Geosystems*, 12(7), 1–23, doi:10.1029/2011GC003577, 2011.
- 1323 Palomeras, I., Villaseñor, A., Thurner, S., Levander, A., Gallart, J. and Harnafi, M.: Lithospheric
1324 structure of Iberia and Morocco using finite-frequency Rayleigh wave tomography from
1325 earthquakes and seismic ambient noise, *Geochemistry, Geophys. Geosystems*, 1–17,
1326 doi:10.1002/2016GC006657, 2017.
- 1327 Pedreira, D., Pulgar, J. A., Gallart, J. and Díaz, J.: Seismic evidence of Alpine crustal thickening
1328 and wedging from the western Pyrenees to the Cantabrian Mountains (north Iberia), *J.*
1329 *Geophys. Res.*, 108(B4), 1–21, doi:10.1029/2001JB001667, 2003.
- 1330 Pereira, M. F., Chichorro, M., Williams, I. S., Silva, J. B., Fernández, C., Diaz-Azpiroz, M., Apraiz,

- 1331 A. and Castro, A.: Variscan intra-orogenic extensional tectonics in the Ossa – Morena-Évora –
 1332 Aracena – Lora del Río metamorphic belt , SW Iberian Zone (E Massif): SHRIMP zircon U – Th –
 1333 Pb geochronology, in *Ancient Orogens and Modern Analogues*, edited by J. B. Murphy, J. D.
 1334 Keppie, and A. J. Hynes, pp. 327, 215–237, Geological Society of London, Special Publications.,
 1335 2009.
- 1336 Pereira, M. F., Ribeiro, C., Vilallonga, F., Chichorro, M., Drost, K., Silva, J. B., Albardeiro, L.,
 1337 Hofmann, M. and Linnemann, U.: Variability over time in the sources of South Portuguese Zone
 1338 turbidites: Evidence of denudation of different crustal blocks during the assembly of Pangaea,
 1339 *Int. J. Earth Sci.*, 103(5), 1453–1470, doi:10.1007/s00531-013-0902-8, 2014.
- 1340 Pérez-Cáceres, I., Martínez Poyatos, D., Simancas, J. F. and Azor, A.: The elusive nature of the
 1341 Rhenic Ocean suture in SW Iberia, *Tectonics*, 34(12), 2429–2450, doi:10.1002/2015TC003947,
 1342 2015.
- 1343 Pérez-Cáceres, I., Simancas, J. F., Martínez Poyatos, D., Azor, A. and González Lodeiro, F.:
 1344 Oblique collision and deformation partitioning in the SW Iberian Variscides, *Solid Earth*, 7(3),
 1345 857–872, doi:10.5194/se-7-857-2016, 2016.
- 1346 Pérez-Estaún, A., Bastida, F., Alonso, J. L., Marquínez, J., Aller, J., Alvarez-Marrón, J., Marcos, A.
 1347 and Pulgar, J. A.: A thin-skinned tectonics model for an arcuate fold and thrust belt: The
 1348 Cantabrian Zone (Variscan Ibero-Armorican Arc), *Tectonics*, 7(3), 517–537,
 1349 doi:https://doi.org/10.1029/TC007i003p00517, 1988.
- 1350 Pérez-Estaún, A., Bastida, F., Martínez Catalán, J.R. Gutierrez Marco, J. C., Marcos, A. and
 1351 Pulgar, J. .: West Asturian-Leonese Zone. Stratigraphy, in *Pre-Mesozoic Geology of Iberia*,
 1352 edited by E. Dallmeyer, R.D. and Martínez Garcia, pp. 92–102, Springer-Verlag, Berlin., 1990.
- 1353 Pérez-Estaún, A., Martínez Catalán, J. R. and Bastida, F.: Crustal thickening and deformation
 1354 sequence in the footwall to the suture of the Variscan belt of northwest Spain, *Tectonophysics*,
 1355 191(3–4), 243–253, doi:10.1016/0040-1951(91)90060-6, 1991.
- 1356 Pérez-Estaún, A., Pulgar, J. A., Banda, E. and Alvarez-Marrón, J.: Crustal structure of the
 1357 external variscides in northwest Spain from deep seismic reflection profiling, *Tectonophysics*,
 1358 232(1–4), doi:10.1016/0040-1951(94)90078-7, 1994.
- 1359 Pin, C., Fonseca, P. E., Paquette, J. L., Castro, P. and Matte, P.: The ca. 350 Ma Beja Igneous
 1360 Complex: A record of transcurrent slab break-off in the Southern Iberia Variscan Belt?,
 1361 *Tectonophysics*, 461(1–4), 356–377, doi:10.1016/j.tecto.2008.06.001, 2008.
- 1362 Pulgar, J. A., Gallart, J., Fernández-Viejo, G., Pérez-Estaún, A. and Álvarez-Marrón, J.: Seismic
 1363 image of the Cantabrian Mountains in the western extension of the Pyrenees from integrated
 1364 ESCIN reflection and refraction data, *Tectonophysics*, 264(1–4), 1–19, doi:10.1016/S0040-
 1365 1951(96)00114-X, 1996.
- 1366 Quesada, C. and Dallmeyer, R. D.: Tectonothermal evolution of the Badajoz-Córdoba shear
 1367 zone (SW Iberia): characteristics and ⁴⁰Ar/³⁹Ar mineral age constraints, *Tectonophysics*,
 1368 231(1–3), 195–213, doi:10.1016/0040-1951(94)90130-9, 1994.
- 1369 Quintana, L., Pulgar, J. A. and Alonso, J. L.: Displacement transfer from borders to interior of a
 1370 plate: A crustal transect of Iberia, *Tectonophysics*, 663, 378–398,
 1371 doi:10.1016/j.tecto.2015.08.046, 2015.
- 1372 Rat, P.: The Basque-Cantabrian basin between the Iberian and European plates: Some facts but
 1373 still many problems, *Rev. la Soc. Geológica España*, 1(3–4), 327–348, 1988.

- 1374 Reche, J., Martínez, F. J., Arboleya, M. L., Dietsch, C. and Briggs, W. D.: Evolution of a kyanite-
1375 bearing belt within a HT-LP orogen: the case of NW Variscan Iberia, *J. Metamorph. Geol.*, 16(3),
1376 379–394, doi:10.1111/j.1525-1314.1998.00142.x, 1998.
- 1377 Robardet, M.: Alternative approach to the Variscan Belt in southwestern Europe: Preorogenic
1378 paleobiogeographical constraints, *Spec. Pap. Geol. Soc. Am.*, 364, 1–15, doi:10.1130/0-8137-
1379 2364-7.1, 2002.
- 1380 Robardet, M. and Gutiérrez Marco, J. C.: Ossa-Morena Zone. Stratigraphy. Passive Margin
1381 Phase (Ordovician-Silurian-Devonian), in *Pre-Mesozoic Geology of Iberia*, edited by R. D.
1382 Dallmeyer and E. Martínez García, pp. 267–272, Springer-Verlag, Berlin., 1990.
- 1383 Rodrigues, B., Chew, D. M., Jorge, R. C. G. S., Fernandes, P., Veiga-Pires, C. and Oliveira, J. T.:
1384 Detrital zircon geochronology of the Carboniferous Baixo Alentejo Flysch Group (South
1385 Portugal); Constraints on the provenance and geodynamic evolution of the South Portuguese
1386 Zone, *J. Geol. Soc. London.*, 172, 294–308, doi:10.1144/jgs2013-084, 2015.
- 1387 Ross, A. R., Brown, L. D., Pananont, P., Nelson, K. D., Klemperer, S. L., Haines, S., Wenjin, Z. and
1388 Jingru, G.: Deep reflection surveying in central Tibet: Lower-crustal layering and crustal flow,
1389 *Geophys. J. Int.*, 156(1), 115–128, doi:10.1111/j.1365-246X.2004.02119.x, 2004.
- 1390 Royden, L.: Coupling and decoupling of crust and mantle in convergent orogens: Implications
1391 for strain partitioning in the crust, *J. Geophys. Res.*, 101(B8), 17679–17705, 1996.
- 1392 Rubio Pascual, F. J., Arenas, R., Martínez Catalán, J. R., Rodríguez Fernández, L. R. and
1393 Wijbrans, J. R.: Thickening and exhumation of the Variscan roots in the Iberian Central System:
1394 Tectonothermal processes and $40\text{Ar}/39\text{Ar}$ ages, *Tectonophysics*, 587, 207–221,
1395 doi:10.1016/j.tecto.2012.10.005, 2013.
- 1396 Sánchez-García, T., Quesada, C., Bellido, F., Dunning, G. R. and González del Tánago, J.: Two-
1397 step magma flooding of the upper crust during rifting: The Early Paleozoic of the Ossa Morena
1398 Zone (SW Iberia), *Tectonophysics*, 461(1–4), 72–90, doi:10.1016/j.tecto.2008.03.006, 2008.
- 1399 Sánchez-García, T., Bellido, F., Pereira, M. F., Chichorro, M., Quesada, C., Pin, C. and Silva, J. B.:
1400 Rift-related volcanism predating the birth of the Rheic Ocean (Ossa-Morena zone, SW Iberia),
1401 *Gondwana Res.*, 17(2–3), 392–407, doi:10.1016/j.gr.2009.10.005, 2010.
- 1402 Sánchez de Posada, L. C., Martínez Chacón, M. L., Méndez Fernández, C., Menéndez Alvarez,
1403 J.R. Truyols, J. and Villa, E.: Carboniferous Pre-Stephanian rocks of the Asturian-Leonese
1404 Domain (Cantabrian Zone), in *Pre-Mesozoic Geology of Iberia*, edited by R. D. Dallmeyer and E.
1405 Martínez García, pp. 24–33, Springer-Verlag., 1990.
- 1406 Sánchez Martínez, S., Arenas, R., Andonaegui, P., Martínez Catalán, J. R. and Pearce, J. A.:
1407 Geochemistry of two associated ophiolites from the Cabo Ortegal Complex (Variscan belt of
1408 NW Spain), *Mem. Geol. Soc. Am.*, 200(23), 445–467, doi:10.1130/2007.1200(23), 2007.
- 1409 Schmelzbach, C., Juhlin, C., Carbonell, R. and Simancas, J. F.: Prestack and poststack migration
1410 of crooked-line seismic reflection data: A case study from the South Portuguese Zone fold belt,
1411 southwestern Iberia, *Geophysics*, 72(2), 9–18, doi:10.1190/1.2407267, 2007.
- 1412 Schmelzbach, C., Simancas, J. F., Juhlin, C. and Carbonell, R.: Seismic reflection imaging over
1413 the South Portuguese Zone fold-and-thrust belt, SW Iberia, *J. Geophys. Res. Solid Earth*, 113(8),
1414 1–16, doi:10.1029/2007JB005341, 2008.
- 1415 Seyferth, M. and Henk, A.: Syn-convergent exhumation and lateral extrusion in continental

- 1416 collision zones - Insights from three-dimensional numerical models, *Tectonophysics*, 382(1–2),
1417 1–29, doi:10.1016/j.tecto.2003.12.004, 2004.
- 1418 Shelley, D. and Bossière, G.: A new model for the Hercynian Orogen of Gondwanan France and
1419 Iberia, *J. Struct. Geol.*, 22(6), 757–776, doi:10.1016/S0191-8141(00)00007-9, 2000.
- 1420 Simancas, J. F., Martínez Poyatos, D., Expósito, I., Azor, A. and González Lodeiro, F.: The
1421 structure of a major suture zone in the SW Iberian massif: The Ossa-Morena/central Iberian
1422 contact, *Tectonophysics*, 332(1–2), 295–308, doi:10.1016/S0040-1951(00)00262-6, 2001.
- 1423 Simancas, J. F., Carbonell, R., González Lodeiro, F., Pérez-Estaún, A., Juhlin, C., Ayarza, P.,
1424 Kashubin, A., Azor, A., Martínez Poyatos, D., Almodóvar, G. R., Pascual, E., Sáez, R. and
1425 Expósito, I.: Crustal structure of the transpressional Variscan orogen of SW Iberia: SW Iberia
1426 deep seismic reflection profile (IBERSEIS), *Tectonics*, 22(6), doi:10.1029/2002TC001479, 2003.
- 1427 Simancas, J. F., Carbonell, R., Gonzalez Lodeiro, F., Pérez-Estaún, A., Juhlin, C., Ayarza, P.,
1428 Kashubin, A., Azor, A., Martínez Poyatos, D., Saez, R., Almodovar, G. R., Pascual, E., Flecha, I.
1429 and Marti, D.: Transpressional collision tectonics and mantle plume dynamics: the Variscides of
1430 southwestern Iberia, *Geol. Soc. London, Mem.*, 32(1), 345–354, 2006.
- 1431 Simancas, J. F., Ayarza, P., Azor, A., Carbonell, R., Martínez Poyatos, D., Pérez-Estaún, A. and
1432 González Lodeiro, F.: A seismic geotraverse across the Iberian Variscides: Orogenic shortening,
1433 collisional magmatism, and orocline development, *Tectonics*, 32(3), 417–432,
1434 doi:10.1002/tect.20035, 2013.
- 1435 Snelson, C. M., Randy Keller, G., Miller, K. C., Rumpel, H. M. and Prodehl, C.: Regional Crustal
1436 Structure Derived from the CD-ROM 99 Seismic Refraction/Wide-Angle Reflection Profile: The
1437 Lower Crust and Upper Mantle, in *The Rocky Mountain Region: An Evolving Lithosphere:*
1438 *Tectonics, Geochemistry, and Geophysics*, pp. 271–291., 2013.
- 1439 Spear, F. S.: *Metamorphic Phase Equilibria and pressure-temperature-time paths*, Monograph.,
1440 edited by M. Mineralogical Society of America, Chelsea., 1993.
- 1441 Stille, H.: *Grundfragen der Vergleichenden. Tectonik*, Gebrueder Borntragen, Berlin., 1924.
- 1442 Taner, M. T. and Sheriff, R. E.: Application of Amplitude, Frequency, and Other Attributes to
1443 Stratigraphic and Hydrocarbon Determination, in *AAPG Memoir, Seismic Stratigraphy —*
1444 *Applications to Hydrocarbon Exploration*, vol. 26, pp. 301–327., 1977.
- 1445 Teixell, A., Labaume, P., Ayarza, P., Espurt, N., de Saint Blanquat, M. and Lagabrielle, Y.: Crustal
1446 structure and evolution of the Pyrenean-Cantabrian belt: A review and new interpretations
1447 from recent concepts and data, *Tectonophysics*, 724–725(July 2017), 146–170,
1448 doi:10.1016/j.tecto.2018.01.009, 2018.
- 1449 Truyols, J., Arbizu, M., Garcia-Alcalde, J. L., Garcia-López, S., Mendez-Bendia, I., Soto, F. and
1450 Truyols, M.: The Asturian-Leonese Domain (Cantabrian Zone), in *Pre-Mesozoic Geology of*
1451 *Iberia*, edited by R. D. Dallmeyer and E. Martínez García, pp. 10–19, Springer-Verlag., 1990.
- 1452 de Vicente, G., Giner, J. L., Muñoz-Martí, A., González-Casado, J. M. and Lindo, R.:
1453 Determination of present-day stress tensor and neotectonic interval in the Spanish Central
1454 System and Madrid Basin, central Spain, *Tectonophysics*, 266(1–4), 405–424,
1455 doi:10.1016/S0040-1951(96)00200-4, 1996.
- 1456 Villaseca, C., Orejana, D. and Belousova, E. A.: Recycled metagneous crustal sources for S- and
1457 I-type Variscan granitoids from the Spanish Central System batholith: Constraints from Hf

1458 isotope zircon composition, *Lithos*, 153, 84–93, doi:10.1016/j.lithos.2012.03.024, 2012.

1459 Wever, T.: The Conrad discontinuity and the top of the reflective lower crust-do they
 1460 coincide?, *Tectonophysics*, 157(1–3), 39–58, doi:10.1016/0040-1951(89)90339-9, 1989.

1461 Xiaobo, H. and Tae Kyung, H.: Evidence for strong ground motion by waves refracted from the
 1462 Conrad discontinuity, *Bull. Seismol. Soc. Am.*, 100(3), 1370–1374, doi:10.1785/0120090159,
 1463 2010.

1464

1465

1466 Table 1: Acquisition parameters of the NI seismic profiles shown from figures 3 to 8 and
 1467 former processing flows. These are grouped according to their similarities.

| 1468 | Acquisition parameters | ESCIN-1 (onshore) | ESCIN-2 (onshore) |
|------|-------------------------------|---|--------------------------|
| 1469 | Source | Dynamite-single-hole | Dynamite-single-hole |
| 1470 | Charge | 20 kg at 24 m depth | 20 kg at 24 m depth |
| 1471 | Trace Interval | 60 m | 60 m |
| 1472 | # of traces | 240 | 240 |
| 1473 | Spread configuration | Symmetrical Split-spread | Symmetrical Split-spread |
| 1474 | Fold | 30 | 30 |
| 1475 | Geophones per group | 18 | 18 |
| 1476 | Spread length | 14.5 km | 14.5 km |
| 1477 | Sample rate | 4 ms | 4 ms |
| 1478 | Kirchoff time migration | 5600 m/s | 5600 m/s |
| 1479 | | | |
| 1480 | | ESCIN-3.2 and ESCIN-3.3 (offshore) | |
| 1481 | | | |
| 1482 | Source | Airgun (5490 cu.in) | |
| 1483 | Shot spacing | 75 m | |
| 1484 | Receiver interval | 12.5 m | |
| 1485 | Spread length | 4500 m | |
| 1486 | Fold | 30 | |
| 1487 | Internal offset | 240 m | |
| 1488 | Sample rate | 4 ms | |
| 1489 | Record length | 20 s | |
| 1490 | Kirchoff time migration | 5200 m/s | |
| 1491 | | | |
| 1492 | | IBERSEIS (onshore) | ALCUDIA (onshore) |
| 1493 | | | |
| 1494 | Source | 4, 22T vibrators | 4 (+1), 22T vibrators |
| 1495 | Recording instrument | SERCEL 388, 10 Hz | SERCEL 388, 10 Hz |
| 1496 | # active channels | 240 minimum | 240 minimum |
| 1497 | Station spacing | 35 m | 35 m |
| 1498 | Station configuration | 12 geophones | 12 geophones |
| 1499 | Source spacing | 70 m | 70 m |
| 1500 | Sweep frequencies | non-linear 8-80 Hz | non-linear 8-80 Hz |
| 1501 | Sweep length | 20 s | 20 s |
| 1502 | Listening time | 40 s | 40 s |
| 1503 | Sample rate | 2 ms | 4 ms |

| | | | |
|------|-------------------------|-------------------------|-------------------------|
| 1504 | Spread type | Asymmetric split-spread | Asymmetric split-spread |
| 1505 | Nominal fold | 60 (minimum) | 60 (minimum) |
| 1506 | Kirchoff time migration | 6000 m/s | 6200 m/s |

1507
1508
1509
1510

Figure captions

1511 Figure 1: (a) Map of the Iberian Peninsula showing the outcrops of the Variscan basement and
1512 the subdivision in zones of the Iberian Massif. The main strike-slip shear zones, traces of
1513 Variscan folds and gneiss domes are also included. Blue lines show the position of normal
1514 incidence seismic reflection profiles and that of the CIMDEF transect. See legend for
1515 abbreviations. (b) Map of the outcropping granitoids in the Iberian Peninsula together with the
1516 main structures.

1517 Figure 2: Processing flow carried over the SEG-Y original stack sections. This task was
1518 geared to improve and homogenize the resolution of the seismic images while creating
1519 new migrated sections. See Martínez García, (2019) for further details.

1520 Figure 3: Cross-section (a) and depth converted time migrated section ($v=5600$ m/s) along
1521 the NI seismic profile ESCIN-1 (Fig. 1), without (b) and with interpretation (c). A sketch of
1522 the most important features is presented in (d). CDP: Common Depth Point. TWT: Two-way
1523 travel time. WALZ: West Asturian-Leonese Zone. CZ: Cantabrian Zone. The position of the
1524 Narcea Antiform is indicated. Red dashed lines represent the boundaries provided by chaos
1525 and variance attribute analyses. Nomenclature for reflections goes as follows: (ot),
1526 outcropping thrusts; (t), thrusts affecting the basement; (b), indifferiated basement;
1527 (st), sole thrust; (c), top of the lower crust; (ir), lower crust internal reflectivity; (m) is the
1528 Moho; (mig) are curved features resulting from the migration of discontinuous reflections.
1529 Depth conversion is based on migration velocities.

1530 Figure 4: Cross-section ((a) modified from Gallastegui et al., 2016) and depth converted
1531 time migrated section ($v=5600$ m/s) of the NI seismic profile ESCIN-2 (Fig. 1), without (b)
1532 and with interpretation (c). A sketch of the most important features is presented in (d). A
1533 1D velocity profile as modeled from wide-angle data (Pulgar et al., 1996) appears in (e).
1534 CDP: Common Depth Point. TWT: Two-way travel time. CZ: Cantabrian Zone. Some
1535 discontinuous reflections are traced on the basis of their geometry on the stack image
1536 (Pulgar et al., 1996). Red dashed lines represent the boundaries provided by chaos and
1537 variance attribute analyses. (s), sediments; (t), thrusts; (ot), outcropping thrusts; (ps),
1538 Paleozoic sediments; (c), top of the lower crust; (lc), lower crust; (m), Moho. Depth
1539 conversion is based on migration velocities.

1540 Figure 5: Cross-section (a) and depth converted time migrated section ($v=5200$ m/s) of the
1541 NI seismic profile ESCIN-3.3 (Fig. 1), without (b) and with interpretation (c). A sketch of the
1542 most important features is presented in (d). A 1D velocity profile as modeled from wide-
1543 angle data (Ayarza et al., 1998) in presented in (e). CDP: Common Depth Point. TWT: Two-
1544 way travel time. CZ: Cantabrian Zone. WALZ: West Asturian-Leonese Zone. CIZ: Central
1545 Iberian Zone. The offshore projection of the Viveiro Fault is indicated. Red dashed lines
1546 represent the boundaries provided by chaos and variance attribute analyses. (s),
1547 sediments; (t), thrusts; (st), sole thrust; (ef), extensional features; (c), top of the lower

1548 crust; (lc), lower crust; (ir) lower crust internal reflectivity; (m), Moho; (sc), subcrustal
1549 reflections; (mig) curved features resulting from the migration of discontinuous reflections.
1550 Depth conversion is based on migration velocities.

1551 Figure 6: Cross-section (a) and depth converted time migrated section ($v=5200$ m/s) of the
1552 NI seismic profile ESCIN-3.2 (Fig. 1), without (b) and with interpretation (c). A sketch of the
1553 most important features is presented in (d). CDP: Common Depth Point. TWT: Two-way
1554 travel time. GTMZ: Galicia-Trás-os-Montes Zone. CIZ: Central Iberian Zone. (s), sediments;
1555 (ef), extensional features; (lc), lower crust; (m), Moho; (sc), subcrustal reflections; (czlc) CZ
1556 underthrust lower crust. Depth conversion is based on migration velocities.

1557 Figure 7: Cross-section ((a) modified from Martínez Poyatos et al., 2012) and depth
1558 converted time migrated section ($v=6200$ m/s) of the NI seismic profile ALCUDIA (Fig. 1),
1559 without (b) and with interpretation (c). A sketch of the most important features is
1560 presented in (d). A 1D velocity profile as modeled from wide-angle data (Palomeras et al.,
1561 in press) is overlapped in (d). CDP: Common Depth Point. TWT: Two-way travel time. CIZ:
1562 Central Iberian Zone. OMZ: Ossa-Morena Zone. (cu): Central Unit; (vf): vertical folds; (g):
1563 granites; (ef): extensional features; (c): top of the lower crust; (lc): lower crust; (cc) and
1564 (cc'): crocodile structure; (m): Moho. Red dashed lines represent the boundaries provided
1565 by chaos and variance attribute analyses. Depth conversion is based on migration
1566 velocities.

1567 Figure 8: Cross-section ((a), modified from Simancas et al., 2003) and depth converted time
1568 migrated section ($v=6000$ m/s) of the NI seismic profile IBERSEIS (Fig. 1), without (b) and
1569 with interpretation (c). A sketch of the most important features is presented in (d). Two 1D
1570 velocity profiles as modeled from wide-angle data (Palomeras et al., 2009) are overlapped
1571 in (d). CDP: Common Depth Point. TWT: Two-way travel time. CIZ: Central Iberian Zone.
1572 OMZ: Ossa-Morena Zone. SPZ: South Portuguese Zone. (t), thrusts; (ot), outcropping
1573 thrusts; (irb), Iberseis Reflective Body; (c), top of the lower crust; (lc), lower crust; (ir) lower
1574 crust internal reflectivity; (lct), lower crust thrusts; (m), Moho. Depth conversion is based
1575 on migration velocities.

1576 Figure 9: Joint geological interpretation of all the seismic sections (normal incidence and
1577 seismic noise) whose location is shown in figure 1. (a): ESCIN-1, ESCIN3-3 and ESCIN-3.2.
1578 (b): ALCUDIA and IBERSEIS. (c): CIMDEF (Andrés et al., 2020). Special attention should be
1579 paid to the depth and geometry of the Moho and mid-crustal discontinuity. Alpine
1580 structures (i.e. crustal thickening) appear in ESCIN-1 and in CIMDEF. The rest are Variscan
1581 features.

1582 Figure 10: Map of the Moho depth as derived from tomography of shear waves (seismic
1583 noise and earthquakes, Palomeras et al., 2017) with the projection of the seismic profiles
1584 already shown in figure 1 and described along the text. A sketch of the geometry of the
1585 main discontinuities (Moho and Conrad) is also shown.

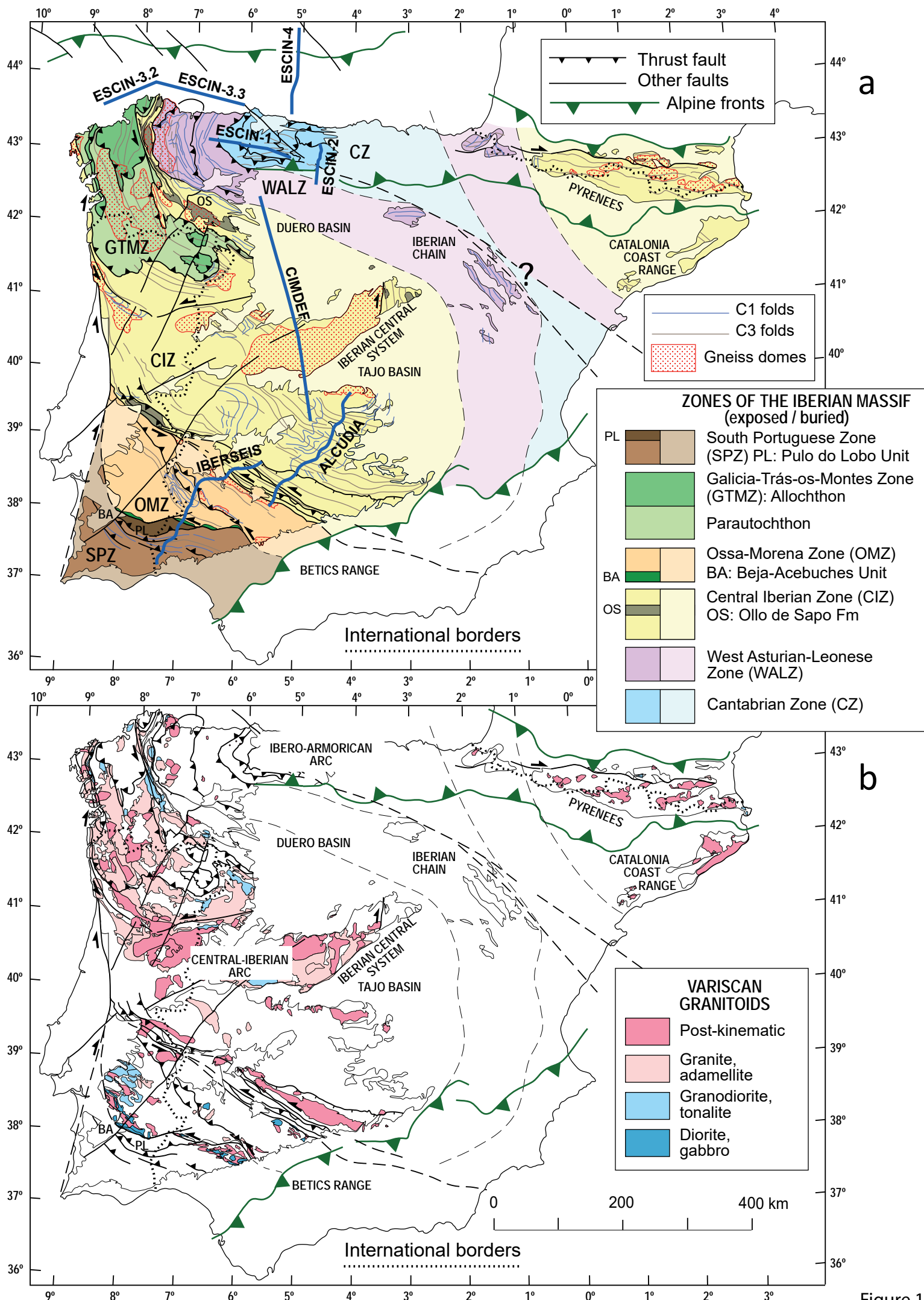


Figure 1

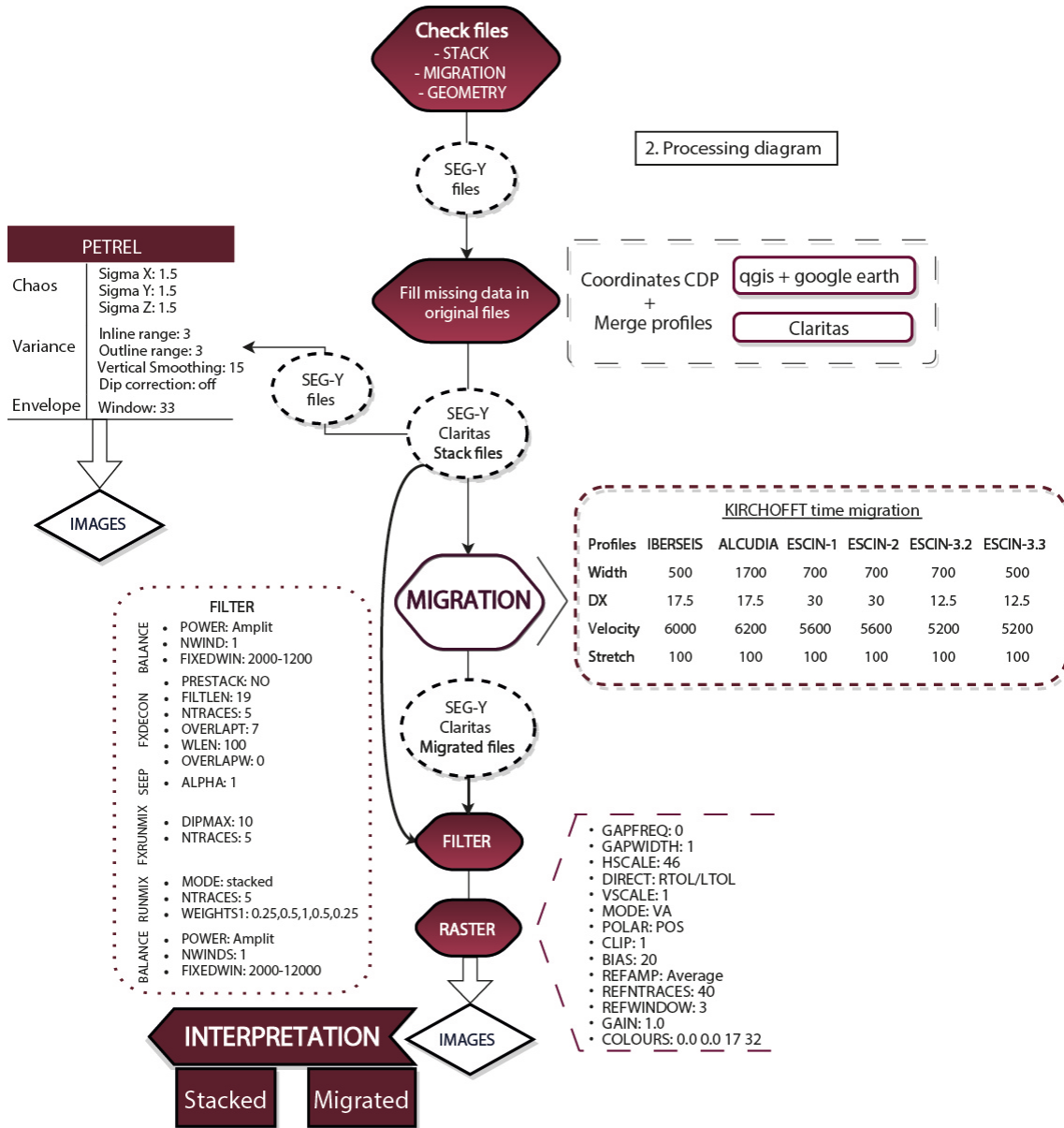


Figure 2

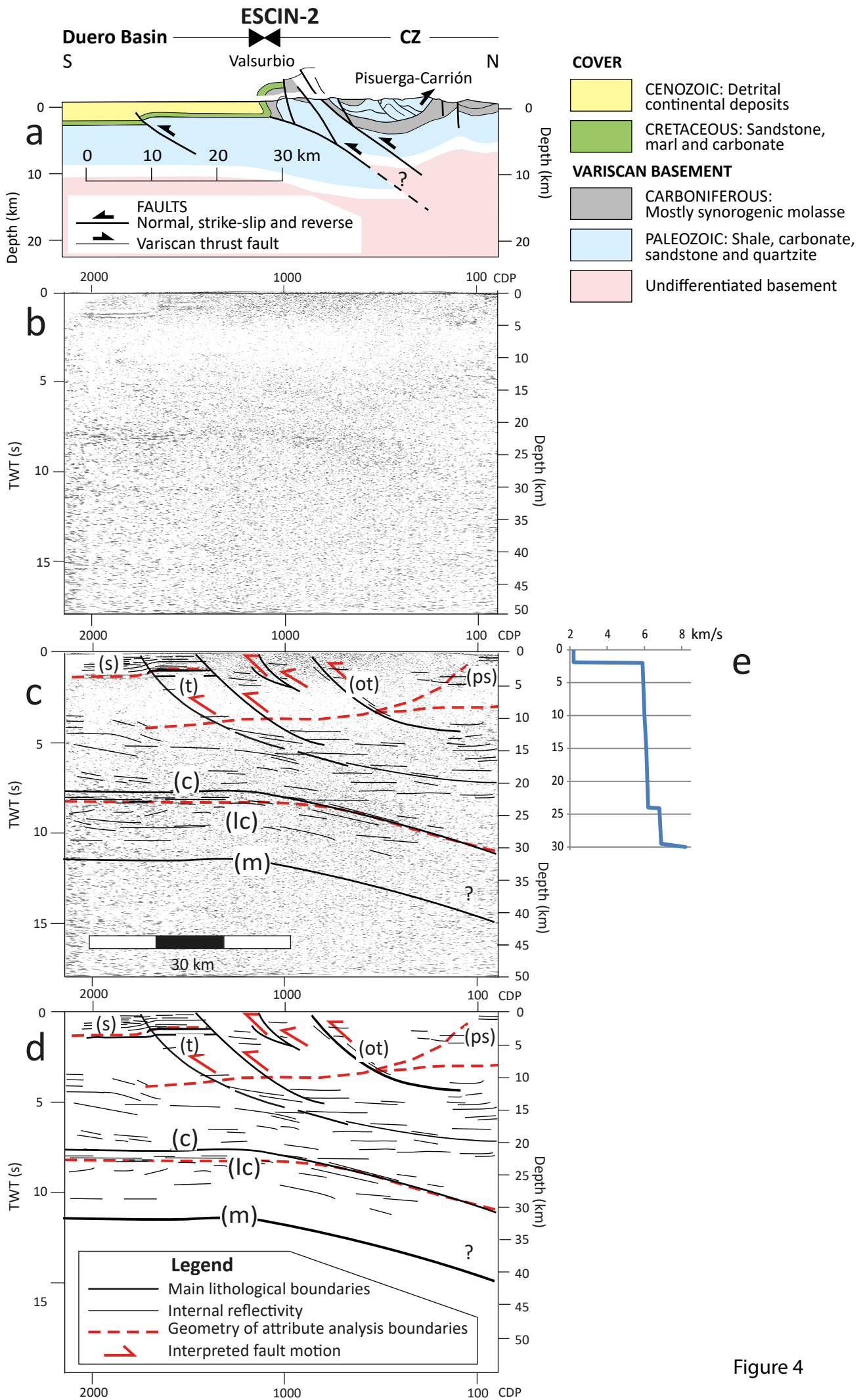


Figure 4

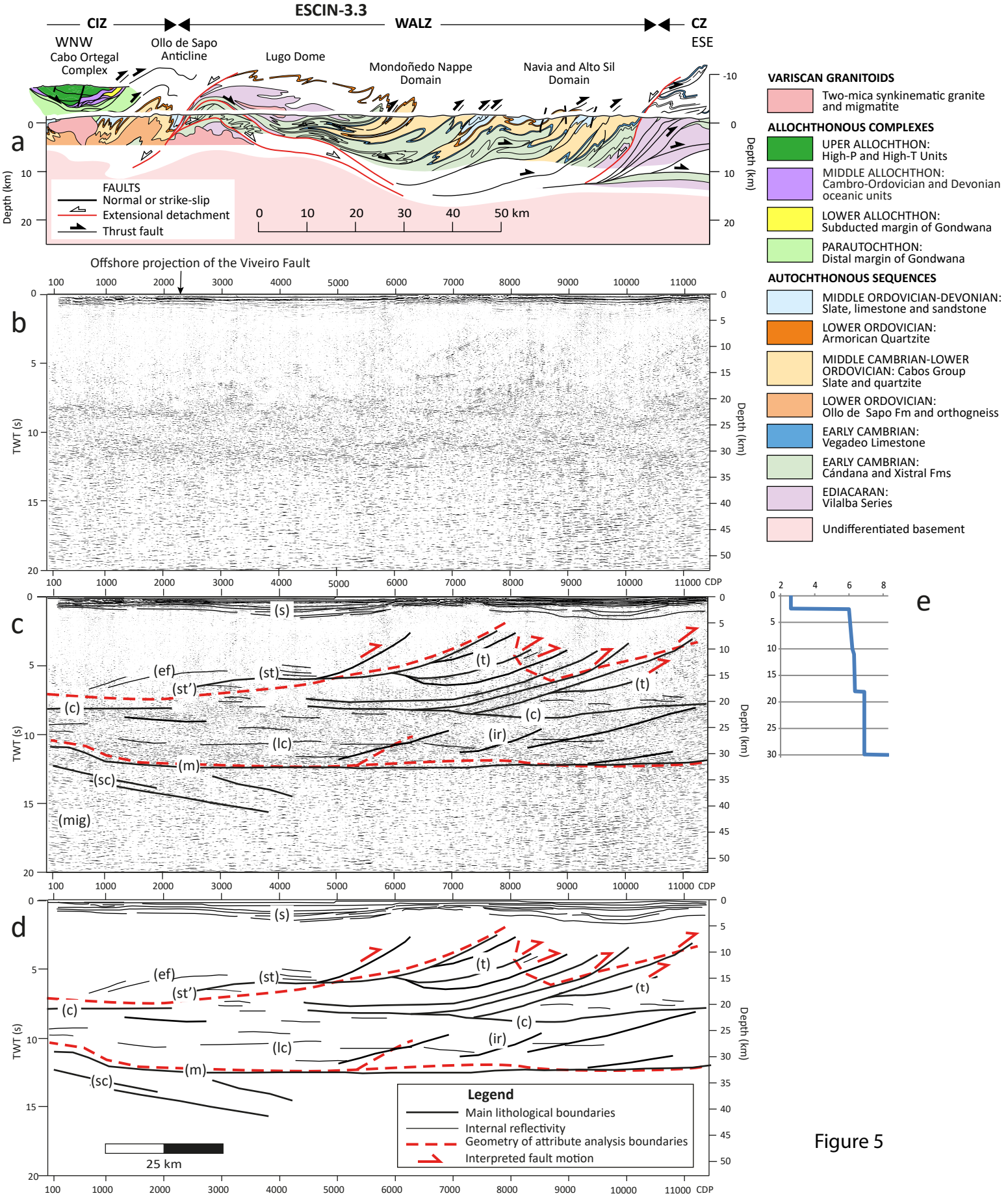


Figure 5

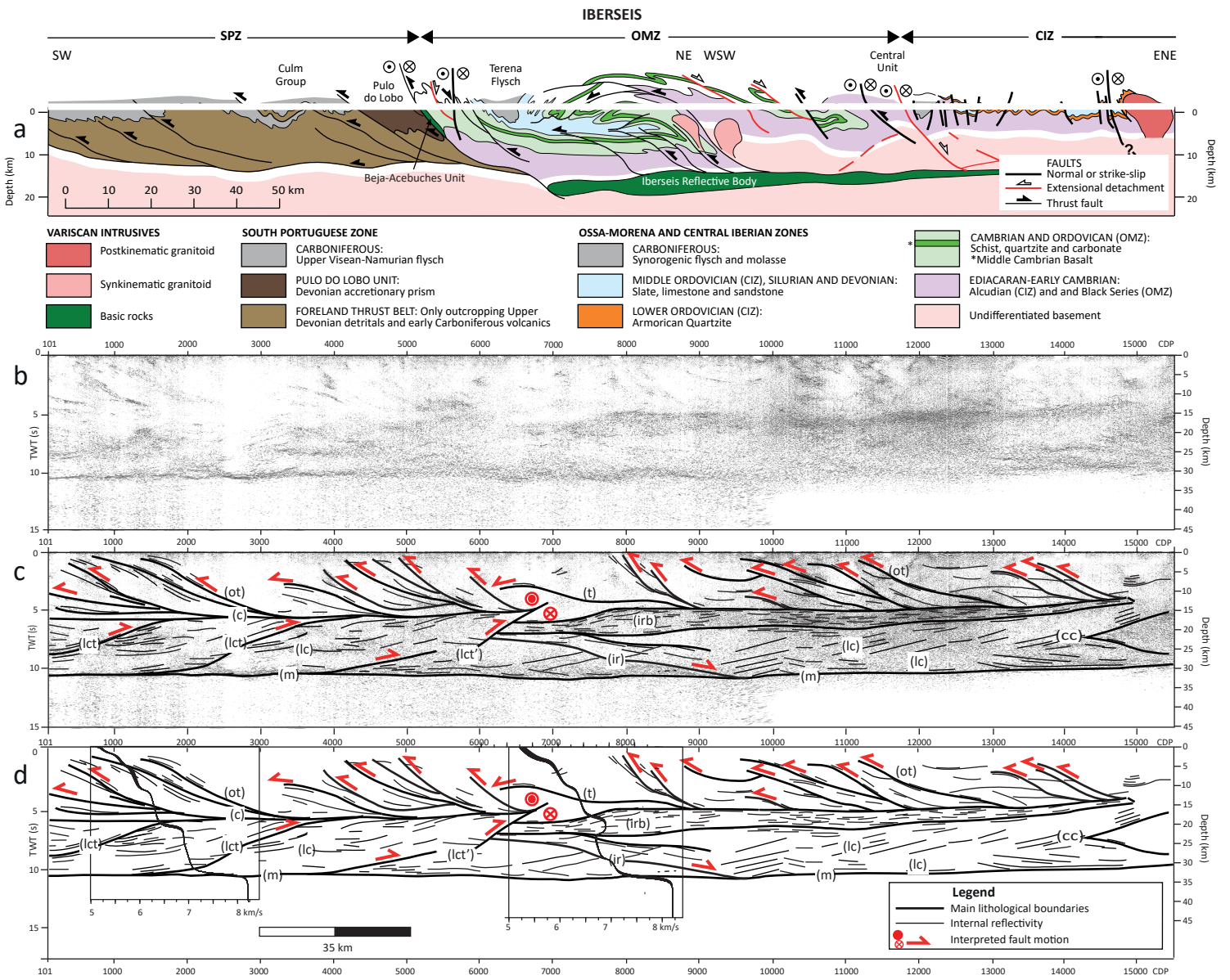


Figure 8

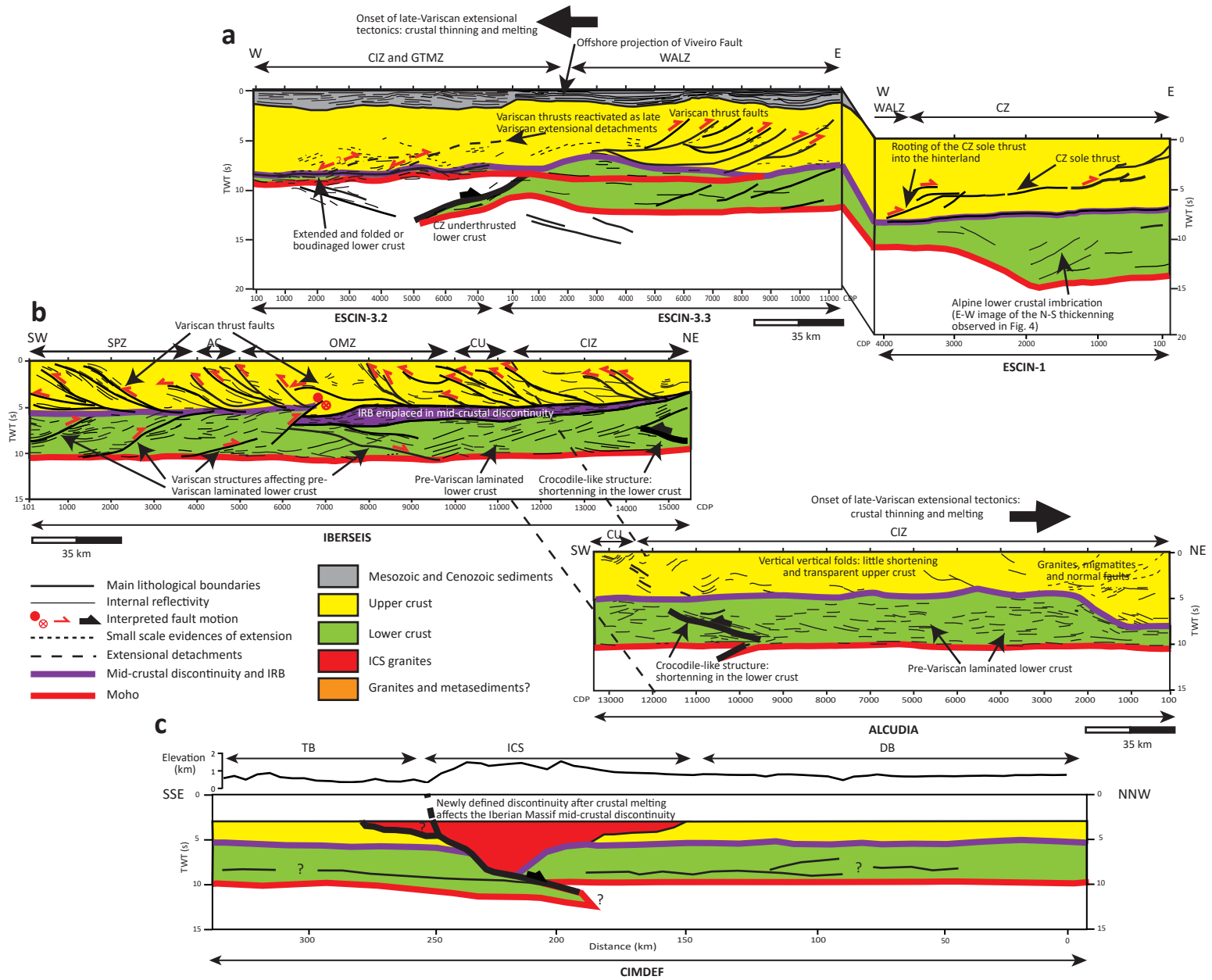


Figure 9

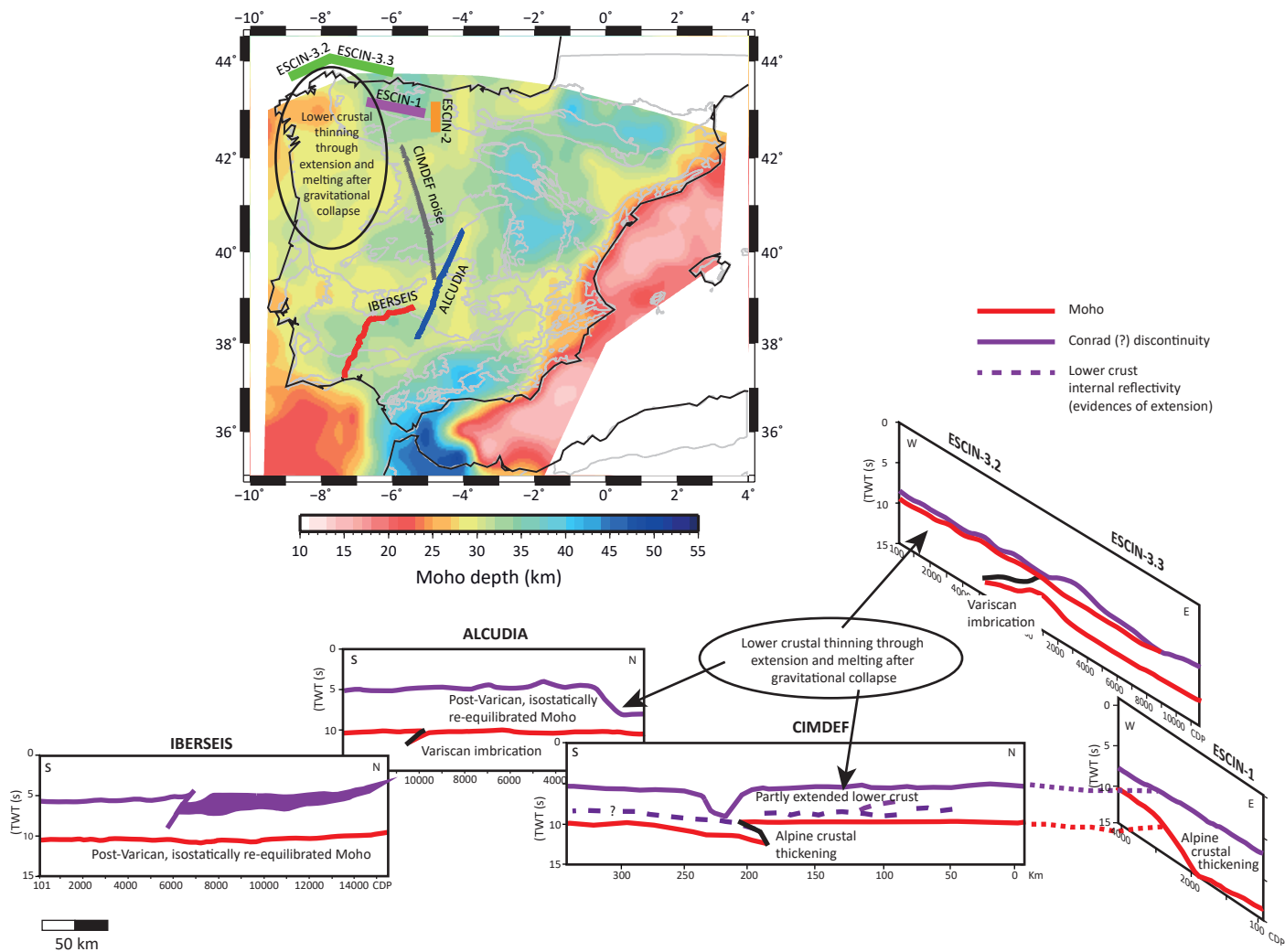


Figure 10